Mixed Sand—Mud Bedforms Produced by Transient Turbulent Flows in the Fringe of Submarine Fans: Indicators of Flow Transformation

Baker, Megan L.; Baas, Jaco H.

Sedimentology

DOI:
10.1111/sed.12714

Published: 01/08/2020

Publisher's PDF, also known as Version of record

SEDIMENTOLOGY the journal of the International Association of Sedimentologists

Sedimentology (2020) **67**, 2645–2671 doi: 10.1111/sed.12714

Mixed sand–mud bedforms produced by transient turbulent flows in the fringe of submarine fans: Indicators of flow transformation

MEGAN L. BAKER[1] and JACO H. BAAS
School of Ocean Sciences, Bangor University, Menai Bridge, Isle of Anglesey, LL59 5AB, UK (E-mail: megan.l.baker@durham.ac.uk)

Associate Editor – Fabrizio Felletti

ABSTRACT

The fringe of fine-grained deep-marine systems often exhibits complex sedimentary facies and facies associations, because the presence of clay promotes the development of transient turbulent flows with complex depositional properties. Relatively little is known about the variation of current-induced sedimentary structures found within these facies. This study provides the first comprehensive description and interpretation of mixed sandstone–mudstone bedforms observed in the fringe of the mud-rich submarine fan that makes up the Aberystwyth Grits Group and Borth Mudstone Formation (Wales, UK). Using textural and structural descriptions, 158 bedforms in sediment gravity flow deposits were characterized into three main types: 'classic' sandy current ripples, large current ripples and low-amplitude bed-waves. The sandy current ripples comprise clean sandstone, with average heights and lengths of 11 mm and 141 mm, respectively. The large current ripples are composed of mixed sandstone–mudstone and possess greater dimensions than the sandy current ripples, with an average height of 19 mm and an average length of 274 mm. The low-amplitude bed-waves are long thin bedforms composed commonly of mixed sandstone–mudstone, with an average height and length of 10 mm and 354 mm, respectively. The large current ripples and low-amplitude bed-waves are strikingly similar to experimental bedforms produced under decelerating mixed sand–mud flows and are interpreted to form beneath transitional flows with enhanced and attenuated near-bed turbulence, respectively. From the fringe to the distal fringe of the fan, the dominant bedform type changed from sandy current ripples, via large current ripples, to low-amplitude bed-waves, suggesting that the flows changed from turbulent to increasingly turbulence-modulated. It is proposed that the flow Reynolds number reduced, reflecting this flow transformation, from a combination of constant or decreasing flow height, flow deceleration from sediment deposition, and increasing flow viscosity due to the shear-thinning nature of clay-rich suspensions. Large current ripples and low-amplitude bed-waves are likely to be common in the fringe of other submarine fans. The presence and spatial trends in mixed sand–mud bedform types may be an important tool in interpreting fan fringe environments.

Keywords Bedforms, cohesion, mixed sand–mud, submarine fans, transitional flows, turbulence modulation.

[1] Present address: Department of Geography, Durham University, South Road, Durham, DH1 3LE, UK

INTRODUCTION

Density currents that carry high concentrations of suspended sediment, i.e. high-density sediment gravity flows, allow large volumes of sediment to be transported from the continent to the deep ocean, thus helping to produce the diverse range of deposits found in modern and ancient submarine fans (Kuenen & Migliorini, 1950; Barker *et al.*, 2008; Baas *et al.*, 2011). The majority of high-density sediment gravity flows should contain mud, composed of clay-sized and silt-sized particles, since mud is one of the most common sediment types in the modern ocean and in oceans in the geological past (Flemming, 2002; Schindler *et al.*, 2015). The role of mud has been shown to be significant in a variety of flows, including sediment gravity flows, since clay particles have the unique ability to modulate turbulence in a predictable manner (Wang & Plate, 1996; Baas & Best, 2002; Baas *et al.*, 2009, 2011). Cohesive clay minerals, when suspended in water, have a surface charge that enables electrostatic forces of attraction between individual particles, leading to the formation of clay flocs and gels (Winterwerp & van Kesteren, 2004). Consisting of pervasive networks of linked clay minerals, clay gels may generate a viscosity and yield strength high enough to attenuate or fully suppress the turbulent forces in the flow (Baas & Best, 2002; Baas *et al.*, 2009; Spearman & Manning, 2017). Baas & Best (2002) showed that increasing the clay concentration in high-density flows causes these flows to change behaviour in a non-linear manner through a range of transitional flow types (Baas *et al.*, 2009, fig. 9). Transformations between these transitional flow types depend on the interplay between the cohesive and turbulent forces (Baas *et al.*, 2009; Sumner *et al.*, 2009). Clay concentration and clay type (Baker *et al.*, 2017) control the cohesive forces, and flow velocity controls the turbulent fluid stresses, which work to break the bonds between clay minerals in flocs and gels.

The balance between the turbulent and cohesive forces in a high-density sediment gravity flow determines the interaction of the flow with the sediment bed and its depositional properties. High-density sediment gravity flows that decelerate over a loose sediment bed may deposit sediment that is shaped into bedforms (e.g. Baas *et al.*, 2016). Analysis of these bedforms and their primary current stratification in core and outcrop enables the reconstruction of depositional processes in ancient sedimentary environments. Many studies have investigated the development and stability of bedforms produced in cohesionless sediment under a variety of flow conditions (e.g. Allen, 1968; see Baas *et al.*, 2016, for a comprehensive list). This has resulted in bedform phase diagrams that define the boundaries between bedform types, based on variables that represent the strength and depth of the flow and the grain size of the sediment (e.g. van Rijn, 1990, 1993; van den Berg & van Gelder, 1993). However, recent studies have demonstrated that adding even small volumes of clay to a sand bed or to a flow produces bedform types with different shapes and sizes compared to those in pure sand (Lowe, 1988; Baas *et al.*, 2011, 2013; Schindler *et al.*, 2015). Thus, applying the knowledge contained in bedform phase diagrams for pure sand in ubiquitous cohesive, mixed sand–mud environments should be done with care.

Laboratory experiments by Baas *et al.* (2011, 2013) investigated the sedimentary structures produced by a decelerated flow composed of sand, silt and clay particles. A number of unique, cohesive, mixed sand–silt–clay bedforms were identified and a new bedform phase diagram was proposed (Baas *et al.*, 2016). These novel bedforms include large current ripples, low-amplitude bed-waves, and scour and intra-scour composite bedforms. The new bedform phase diagram of Baas *et al.* (2016) provides a potential resource to understand ancient sedimentary sequences that formed from rapidly decelerated flows composed of sand, silt and clay. This requires the identification and process interpretation of these novel bedforms in their natural environment. The muddy fringes of fine-grained submarine fans are locations where these cohesive bedforms may be expected to be particularly common.

Fine-grained deep-marine systems are gaining increasing attention as hydrocarbon exploration looks to target reservoirs in mud-rich and mixed sand–mud deep-marine systems, such as offshore West Africa (Sprague *et al.*, 2005) and the Gulf of Mexico (Kane & Pontén, 2012). The facies in the fringe environments of these fine-grained systems have been shown to be complex and contain hybrid event beds (Haughton *et al.*, 2003, 2009; Talling *et al.*, 2004, 2012; Barker *et al.*, 2008; Hodgson, 2009; Kane & Pontén, 2012; Fonnesu *et al.*, 2015; Kane *et al.*, 2017; Spychala *et al.*, 2017; Pierce *et al.*, 2018). However, little work has been done to understand whether the bedforms in these fringe

environments differ from those found in more proximal locations of fine-grained systems.

This study focuses on the fringe region of the submarine fan that makes up the Silurian Aberystwyth Grits Group and the Borth Mudstone Formation in west Wales, UK, and presents the first comprehensive description and interpretation of mixed sandstone–mudstone bedforms in a deep-water environment. The specific objectives were to: (i) fully describe and classify the bedform types observed in the field based on their shape, size, texture and internal stratification; (ii) use the strong link between transitional flow type and bedform type, summarized in the extended bedform phase diagram of Baas *et al.* (2016), to interpret the flow processes that formed the different bedform types identified in the field; (iii) interpret the observed spatial distribution of these bedforms in terms of flow transformation from the fringe to the distal fringe of the fan; and (iv) assess the applicability of mixed sand–mud bedforms in the fringe of other deep-marine systems.

GEOLOGICAL SETTING OF THE ABERYSTWYTH GRITS GROUP AND BORTH MUDSTONE FORMATION

The Silurian Aberystwyth Grits Group (AGG) and Borth Mudstone Formation (BMF) are exposed in coastal cliffs between Cwmtydu and Borth in west Wales, UK (Fig. 1). These outcrops are part of a *ca* 40 km long open synclinal structure, in which palaeoflow directions have been found to be subparallel to the north-east-trending cliff lines (Wood & Smith, 1958; Wilson *et al.*, 1992; Smith, 2004; Talling *et al.*, 2004; Cherns *et al.*, 2006; Fig. 1A). The highly wave-polished nature of the outcrops of the AGG and BMF has allowed for detailed analysis of sedimentary structures, sedimentary facies and facies associations (e.g. Wood & Smith, 1958; Talling *et al.*, 2004).

The AGG and BMF formed during a major phase of extensional faulting in the Welsh Basin and its margins in the upper Llandovery, related to collision of Avalonia with Laurentia at low latitude (Cherns *et al.*, 2006). The extensional faulting accompanied major uplift of the hinterland, which became a source of sediment for the Welsh Basin. This coincided with major subsidence of the Welsh Basin, thus providing accommodation space for the accumulation of sediment gravity flow deposits, including the

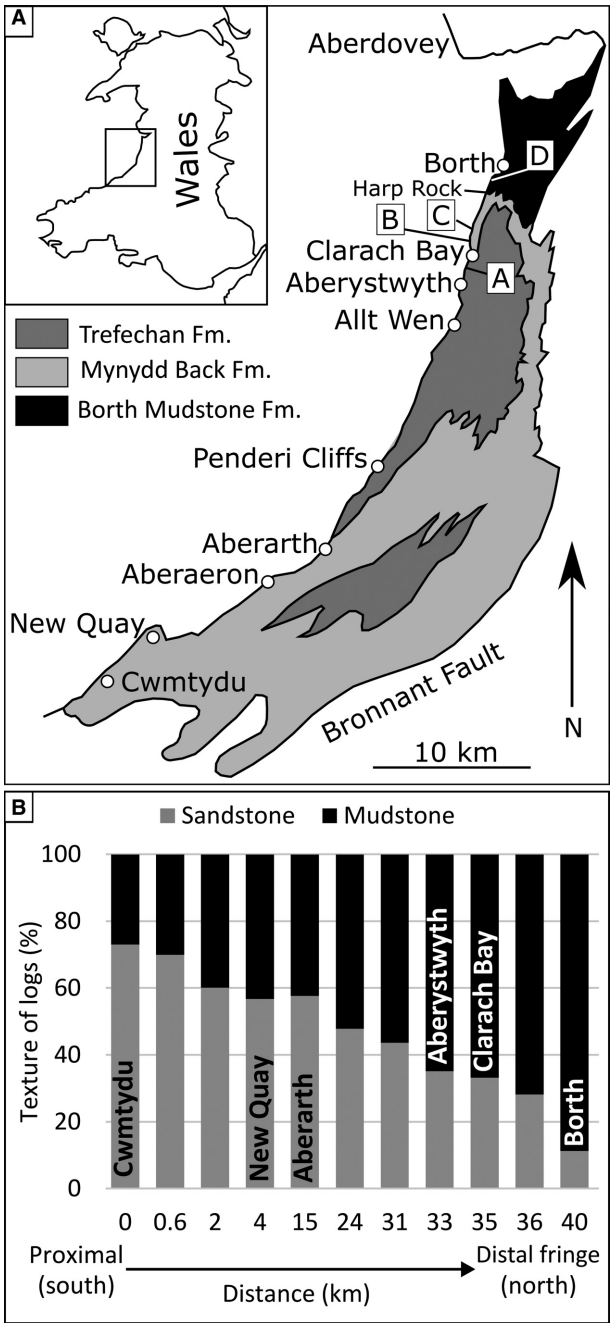

Fig. 1. (A) Geological map of the Aberystwyth Grits Group and Borth Mudstone Formation in Wales (inset). Letters denote position of logs A to D. Modified after Davies *et al.* (1997) and McClelland *et al.* (2011). (B) Changes in the sandstone and mudstone frequency from south to north through the system.

AGG and BMF (Cherns *et al.*, 2006). In the Llandovery, the Welsh Basin was bound by north-east-striking normal faults, which instigated physiographic confinement of the sediment gravity flow deposits (Wilson *et al.*,

1992; Smith, 2004). Previous studies have proposed that most sediment was supplied from the south-west by sediment gravity flows into a linear upper crustal fault trough that was confined to the east and south-east by the Bronnant Fault (Cherns *et al.*, 2006; Gladstone *et al.*, 2018; Fig. 1A). Lovell (1970) subdivided the AGG into the Trefechan and Mynydd Bach formations, which are primarily exposed in the southern and northern part of the coastal outcrops, respectively (Davies *et al.*, 1997; Fig. 1A). The average grain size and the bed thickness of the AGG decrease both north-eastward down the sub-basin and stratigraphically upward (McClelland *et al.*, 2011). The mudstone-rich facies of the BMF have been interpreted to extend laterally and distally beyond the limits of the more sandstone-prone facies of the AGG (Wilson *et al.*, 1992).

The present study comprises field observations from the fringe of the AGG system between Aberystwyth and Harp Rock and the proximal part of the BMF from Harp Rock to Borth (Fig. 1A). The terms 'fringe' and 'distal fringe' are used herein to describe the sub-environments within the studied part of the fan (*cf.* Prélat *et al.*, 2009; Spychala *et al.*, 2017; Fig. 1A). The fringe and distal fringe are represented by average mud percentages of 70% (standard deviation, σ = 7%) and 90% (σ = 2%), respectively (Fig. 1B). The boundary between the fringe and distal fringe is situated approximately at the boundary between the AGG and BMF near Harp Rock (Fig. 1A).

Two distinct types of deposits have been found in the AGG and BMF: (i) sandy and muddy sediment gravity flow deposits; and (ii) interbedded mudstone. The sediment gravity flow facies in the proximal AGG, between Cwmtydu and Aberarth, are a combination of medium-bedded to thick-bedded massive sandstones, muddy sandstones and classical, Bouma-type turbidites (Bouma, 1962; Wilson *et al.*, 1992). Moving distally, north of Aberarth and around Clarach Bay, the massive sandstone units thin and the turbidites primarily contain T_b–T_e or T_c–T_e Bouma-type divisions with occasional, thin T_a divisions, and the interbedded mudstones increase in thickness (Wilson *et al.*, 1992; Fig. 1B). In addition, hybrid event beds are present north of Aberarth (Talling *et al.*, 2004). South of Borth, in the distal fringe of the system, the BMF contains medium to thin-bedded, muddy, mostly T_d–T_e turbidites with thick interbedded mudstones (Wilson *et al.*, 1992; Fig. 1B).

METHODS

Four sedimentary sections were logged in detail at a scale of 1 : 5 between Aberystwyth and Borth across the transition from the AGG to the BMF (Fig. 1A). These logs record a characteristic set of muddy, mixed sandstone–mudstone, and sandy sedimentary facies and facies transitions. Particular attention was given to the vertical and horizontal distribution of heterolithic stratification, mixed sandstone–mudstone bedforms, and couplets of mudstone and underlying thin siltstones. Because of the complex structural deformation within the AGG and BMF, it was not possible to correlate individual beds among the logs. Post-compaction thicknesses of beds normal to bedding were measured using a standard tape measure at an accuracy of 1 mm.

The sedimentary logs were accompanied by detailed descriptions of current-generated bedforms and primary current stratification along the entire outcrop between Aberystwyth and Borth. These descriptions included common bedform types in pure sandstone and novel bedform types in mixed sandstone–mudstone, where cohesive forces were hypothesized to have affected bedform development. The total record consists of 99 mixed sandstone–mudstone bedforms and 59 sandy bedforms. The descriptions of these bedforms are based on high-resolution field photographs, detailed field drawings, granulometric data, and bedform height and length measurements. Grain size was estimated in the field using a hand lens and a grain-size comparator. The colour of the deposits gave an additional indication of the typical grain size, because increasing mud content typically produced darker coloured rock, with black deposits corresponding to mudstone. Strike and dip orientations of bedding planes as well as independent palaeoflow directions from, for example, flute and groove casts were measured using a standard geological compass. If required, these data were used to convert apparent bedform lengths to true bedform lengths using a stereonet. The bedform heights were not corrected for compaction, as the primary porosity of muddy and mixed sandy–muddy sediment is highly variable and cannot easily be reconstructed from sedimentary rocks. However, the angle of cross-lamination observed in sand-rich bedforms was close to the 'angle of repose', suggesting that the degree of compaction for these bedforms was small. The measured heights of the bedforms may slightly

underestimate the heights of the bedforms upon their formation.

Markov chain analysis was conducted to obtain the common facies transitions in the sedimentary logs. Each type of vertical facies transition in the logs was counted to produce a table of observed facies transition counts (Table 1). The probability of the facies transitions was then calculated by dividing the number of occurrences of a facies transition by the sum of all the facies transitions for that facies. The wide range in facies counts for the various facies meant that methods to remove the random probability from the observed probability were unsuitable (e.g. Gingerich, 1969).

SEDIMENTARY FACIES

The sedimentary rocks found within the AGG and BMF are described using a facies scheme, with representative photographs of each facies shown in Fig. 2. Many of the facies observed in this study correspond to facies described in other deep-water sediment gravity flow systems (e.g. Pickering *et al.*, 1986). Figure 3 provides the key to sedimentary logs A, B, C and D (Figs 4 to 7), which demonstrate progressive changes in facies from the fringe to the distal fringe of the fan. Below, each facies is described and their mode of formation is interpreted.

Massive sandstone

Observations

The massive sandstone facies comprises structureless, very fine grained to medium-grained sandstone, which is light blue–grey in colour (Fig. 2A). Most beds lack grading, but some beds show weak to strong normal grading (for example, at 0.04 m, 4.89 m and 5.73 m in Fig. 5). The massive sandstone facies is further characterized by sharp, flat bases and sharp tops or gradually fining-upward transitions. Bed tops are sometimes wavy.

Interpretation

Deposits of massive sand may be formed by rapid suspension fallout from high-concentration sandy gravity flows that are fully turbulent (Arnott & Hand, 1989; Kneller & Branney, 1995; Talling *et al.*, 2012) or transient turbulent (Baas *et al.*, 2009, 2011). The presence of normal grading in the massive sandstone facies is interpreted to represent suspension settling of sand from waning flows (Kneller, 1995). Massive sand may also be generated by *en masse* deposition from sandy gravity flows dominated by laminar flow behaviour, which does not produce normal grading (Shanmugam & Moiola, 1995; Talling *et al.*, 2012). The sharp bed bases suggest an abrupt change in depositional conditions from those producing the underlying bed, as well as possible erosion, which supports the interpretation of rapid input of sediment into the basin by a sediment gravity flow. The sharp tops of the massive sandstone facies indicate another abrupt change in depositional process (e.g. Stevenson *et al.*, 2014); in contrast, the fining-upward transitions suggest a more gradual change in depositional process. The wavy tops of the massive sandstone facies are interpreted to have resulted from post-depositional deformation, possibly involving dewatering after rapid deposition of the sand.

Table 1. Results of the vertical facies transition analysis for the four logs depicted in Figs 4 to 7. Facies in the columns overlie the facies in each row. The value in each cell denotes the probability of the vertical facies transitions. The number in brackets represents the number of transitions of that pair.

	M	Msi	Si	SMh	Smu	Sc	Ss	Sma	Total
M		0.01 (4)	0.73 (223)	0.01 (3)	0.03 (10)	0.00 (0)	0.11 (35)	0.10 (30)	305
Msi	0.56 (5)		0.22 (2)	0.00 (0)	0.00 (0)	0.00 (0)	0.22 (2)	0.00 (0)	9
Si	0.74 (200)	0.02 (5)		0.00 (1)	0.05 (14)	0.00 (0)	0.08 (21)	0.11 (30)	271
SMh	0.57 (8)	0.07 (1)	0.14 (2)		0.00 (0)	0.00 (0)	0.00 (0)	0.21 (3)	14
Smu	0.31 (8)	0.00 (0)	0.42 (11)	0.04 (1)		0.00 (0)	0.23 (6)	0.00 (0)	26
Sc	0.00 (0)	0.00 (0)	0.00 (0)	0.33 (1)	0.00 (0)		0.67 (2)	0.00 (0)	3
Ss	0.54 (38)	0.00 (0)	0.19 (14)	0.04 (3)	0.01 (1)	0.01 (1)		0.21 (15)	72
Sma	0.51 (39)	0.00 (0)	0.21 (16)	0.06 (5)	0.00 (0)	0.03 (2)	0.19 (15)		77

M, mudstone; Msi, silty mudstone; Sc, clast-rich sandstone; Si, siltstone; Sma, massive sandstone; SMh, heterolithic sandstone–mudstone; Smu, structured muddy sandstone; Ss, structured sandstone.

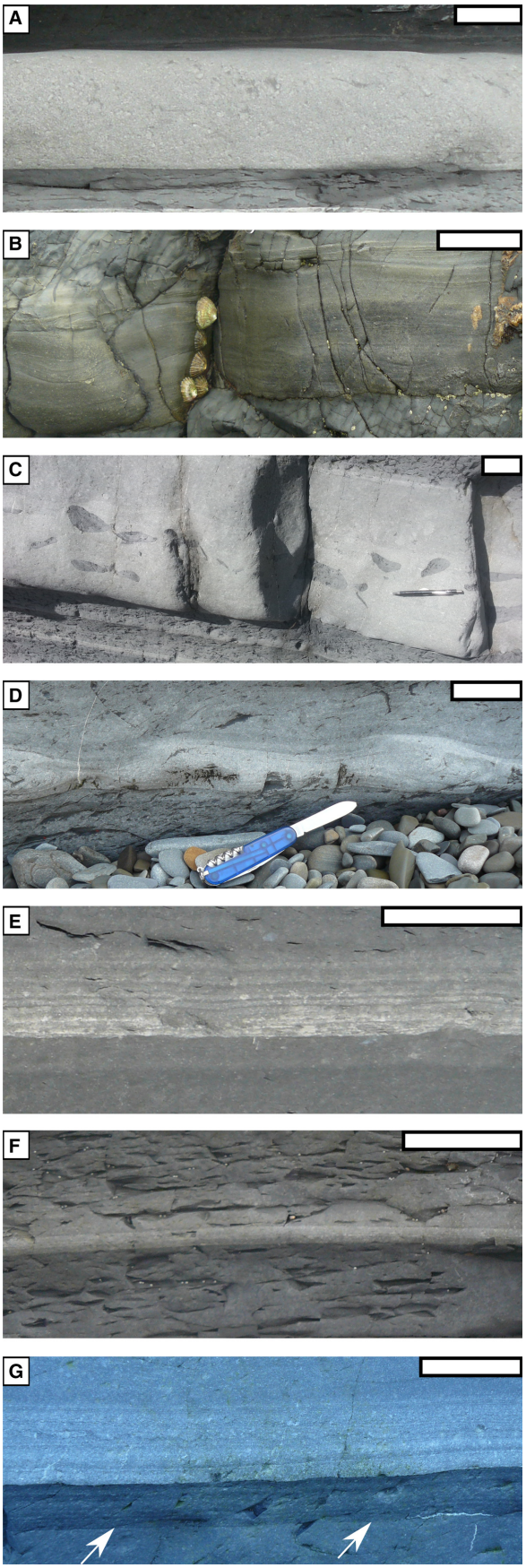

Fig. 2. Representative outcrop photographs of the observed sedimentary facies: (A) massive sandstone; (B) structured sandstone; (C) clast-rich sandstone; (D) structured muddy sandstone, here with large current ripples; (E) heterolithic sandstone–mudstone; (F) siltstone within mudstone; (G) silty mudstone (shown by arrow pointing to the base of the bed). Scale bar is 50 mm long.

Structured sandstone

Observations

The structured sandstone facies consists of light blue–grey, mud-poor, very fine-grained to medium-grained, stratified sandstone (Fig. 2B). Horizontal, plane-parallel lamination is the most common primary current structure (for example, at 0.8 m and 2.88 m in Fig. 4), with subordinate occurrences of wavy lamination (for example, at 2.56 m in Fig. 7) and convoluted lamination (for example, at 4.73 m in Fig. 6), and angle of repose ripple cross-lamination (for example, at 0.14 m and 1.80 m in Fig. 4). Individual laminae are typically up to 3 mm thick. The beds are visually ungraded or normally graded; all beds with convolute lamination lack grading. Bed bases and tops are nearly always sharp and mostly flat, with occasional wavy boundaries. In some instances, the top of structured sandstone facies fine upward and are diffuse.

Interpretation

The presence of primary current lamination in the structured sandstone facies suggests deposition from fully turbulent sandy gravity flows with a lower rate of suspension fall-out than for

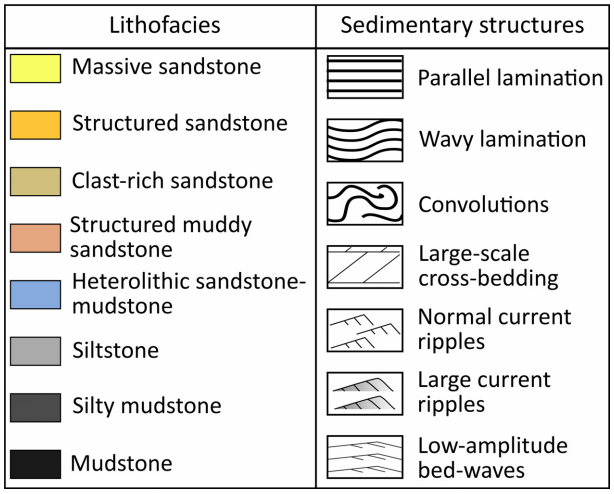

Fig. 3. Key to lithofacies and sedimentary structures, shown in Figs 4 to 8.

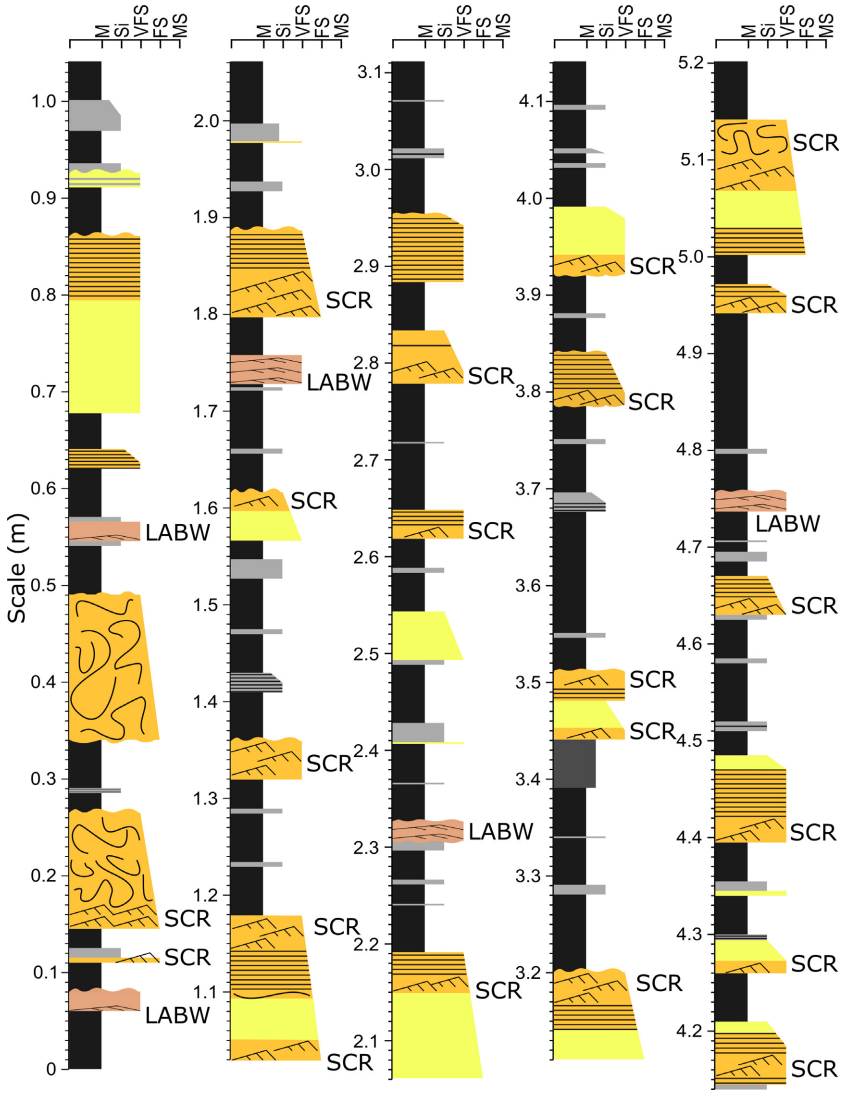

Fig. 4. Sedimentary log A. Position is shown in Fig. 1. LABW, low-amplitude bed-waves; SCR, sandy current ripples. Scale is in metres.

the massive sandstone facies. Current velocity varied, allowing bedload transport to generate upper-stage plane beds and plane-parallel lamination at high velocities, and ripple cross-lamination at low velocities (Allen, 1982; Best & Bridge, 1992). Temporal reduction in flow velocity, and hence flow competence, produced the normally graded beds, whereas ungraded beds suggest a more constant flow velocity or the settling of well-sorted sand. The wavy lamination observed in the structured sandstone facies may have formed by soft sediment deformation of plane-parallel laminae. Some occurrences of wavy lamination also resemble the 'sinusoidal ripple lamination' or 'draped lamination' described by Jopling & Walker (1968) and Ashley *et al.* (1982). These structures have been experimentally shown to form under a flow with high rates of suspension settling depositing over inactive bedforms (Ashley *et al.*, 1982). The convoluted laminae in the Aberystwyth Grits Group formed from deformation of sediment during or shortly after deposition (Gladstone *et al.*, 2018). The observed bed bases and tops in the structured sandstone facies, as well as in all other facies described below, are interpreted in a similar way to the massive sandstone facies.

Clast-rich sandstone

Observations

The clast-rich sandstone facies is light blue–grey, very fine-grained to fine-grained sandstone with dispersed mudstone and matrix-supported black mudstone clasts or light blue–grey, medium-grained sandstone clasts (Fig. 2C). The clast-rich sandstone facies consists of

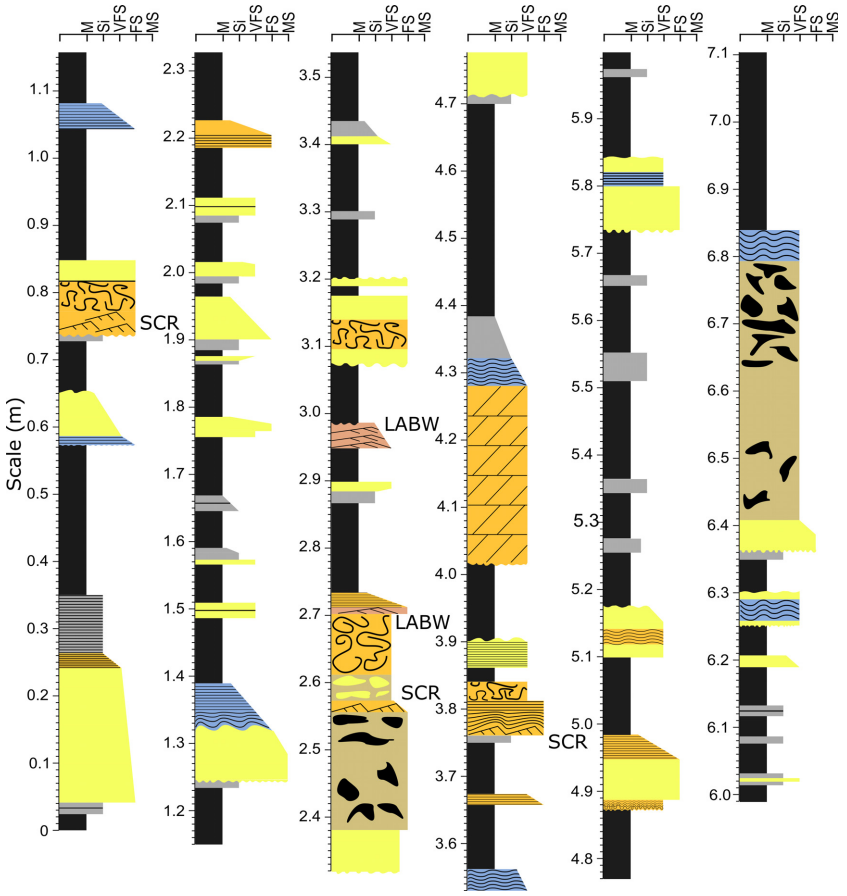

Fig. 5. Sedimentary log B. Position is shown in Fig. 1. LABW, low-amplitude bed-waves; SCR, sandy current ripples. Scale is in metres.

structureless and ungraded beds with sharp, flat bases and tops (for example, at 2.38 m and 6.41 m in Fig. 5). The clasts are well-rounded and have a high aspect ratio with an average length and height of 45 mm and 9 mm, respectively. The clasts were found to have a strong preferred alignment parallel to the bed base. Figure 8I shows that the mean size of the mudstone clasts decreases along the outcrop from Clarach Bay to Borth.

Interpretation

This facies resembles the deposit of a laminar debris flow or an upper-transitional plug flow, in which clay provides the cohesive forces required to support the sand grains and the sand and mud clasts (Iverson, 1997; Baas *et al.*, 2009, 2011; Talling *et al.*, 2012). *En masse* freezing is interpreted to have produced the ungraded, structureless character of these clast-rich beds (Iverson, 1997; Talling *et al.*, 2012). The horizontal alignment of the clasts and their matrix-supported texture provides further evidence that the flow was laminar and cohesive, rather than dominated by turbulence, at the site of deposition. However, the flows could initially have exhibited turbulent behaviour to give the mud and sand clasts a rounded shape after erosion of these clasts from the substrate (Fonnesu *et al.*, 2017). This abrasion process could have helped the change from turbulent flow to laminar flow by the release of clay minerals (Fonnesu *et al.*, 2017). The decreasing mudstone clast size from Clarach Bay to Borth (Fig. 8I) suggests that these clasts disaggregated as the flows travelled through this part of the system.

Structured muddy sandstone

Observations

The structured muddy sandstone facies consists predominantly of mixtures of light blue–grey, very fine-grained to fine-grained sandstone, darker blue–grey mixed sandstone–mudstone, dark blue–grey siltstone and black mudstone (Fig. 2D). The structured character of this facies comprises two bedform types: (i) asymmetrical current ripples with angle of repose cross-

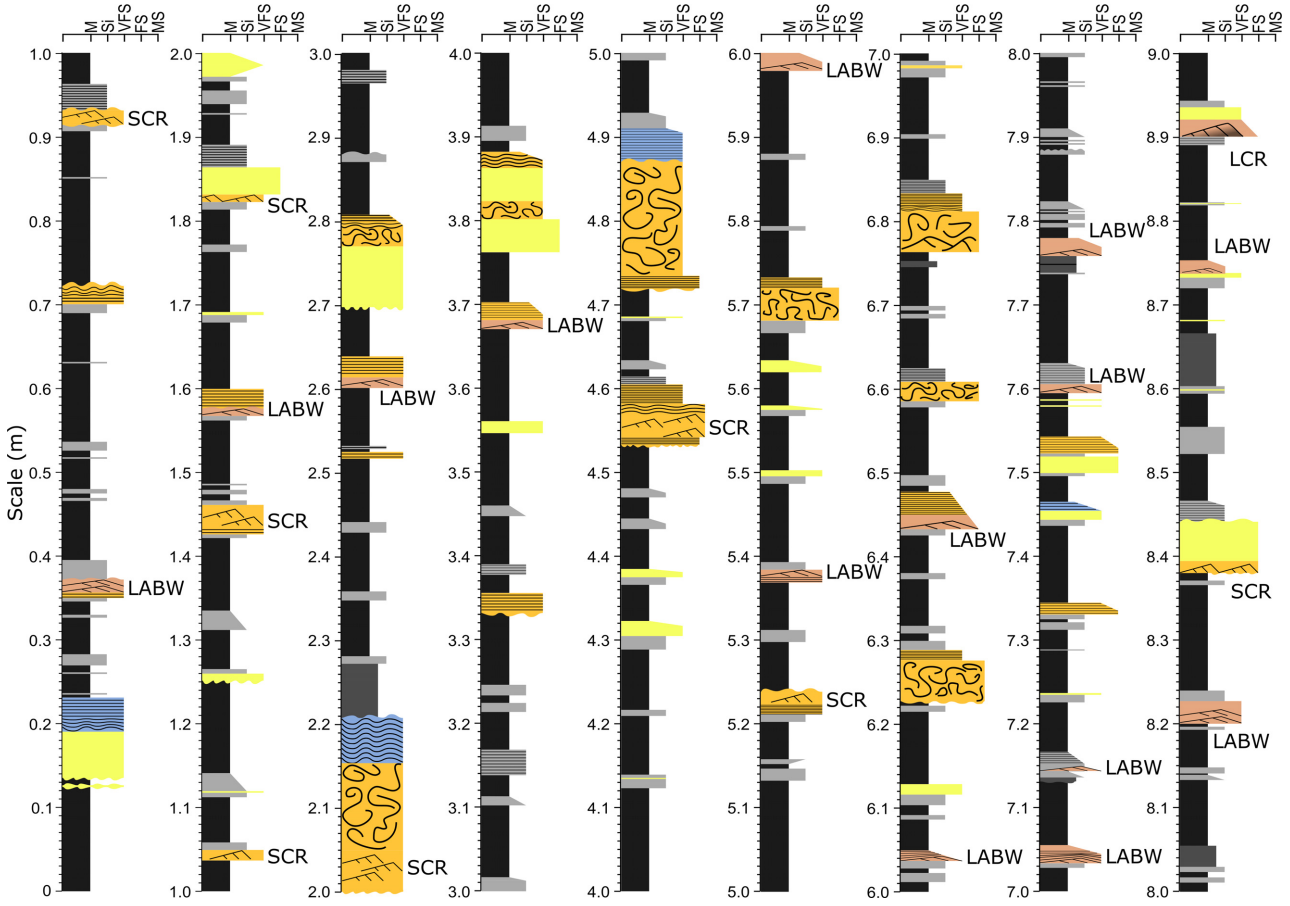

Fig. 6. Sedimentary log C. Position is shown in Fig. 1. LABW, low-amplitude bed-waves; LCR, large current ripples; SCR, sandy current ripples. Scale is in metres.

lamination, generally larger in height and length than the current ripples in the structured sandstone facies, termed *large current ripples* herein (for example, at 0.52 m and 3.99 m in Fig. 7; Fig. 2D); and (ii) thin and long bedforms with low-angle cross-lamination (*ca* 12°), termed *low-amplitude bed-waves* (LABWs) herein (for example, at 2.60 m and 5.98 m in Fig. 6). The large current ripples often climb supercritically, i.e. with climbing angles sufficiently high to preserve the full ripple profiles (Fig. 2D). Most large current ripples are encased in siltstone or mudstone, with this fine-grained sediment forming thick deposits at the base and in the trough of the bedforms, as well as draping the crest and stoss side of the bedforms. The basal mudstone was found to coarsen upward and upstream to sandstone. The LABWs contain varying proportions of sandstone and mudstone, and occasionally climb on top of muddy surfaces. These large current ripples and LABWs are described and compared with 'classic' current ripples in more detail in the section *Sand–mud sedimentary structures*. The bed bases are always sharp and mostly flat, but occasionally wavy. The bed tops are sharp or fine upward as well as flat and occasionally wavy.

Interpretation

The large current ripples in the structured muddy sandstone facies resemble the large bedforms formed below rapidly decelerated turbulence-enhanced transitional flow and lower transitional plug flow in the laboratory, in which high near-bed turbulence causes the height and length of the bedforms to increase compared to sandy current ripples (Baas *et al.*, 2016). The large current ripples climbed supercritically because of high sedimentation rates (Allen, 1971; Jobe *et al.*, 2012), here including clay, silt and sand particles. This agrees with the behaviour of the rapidly decelerated

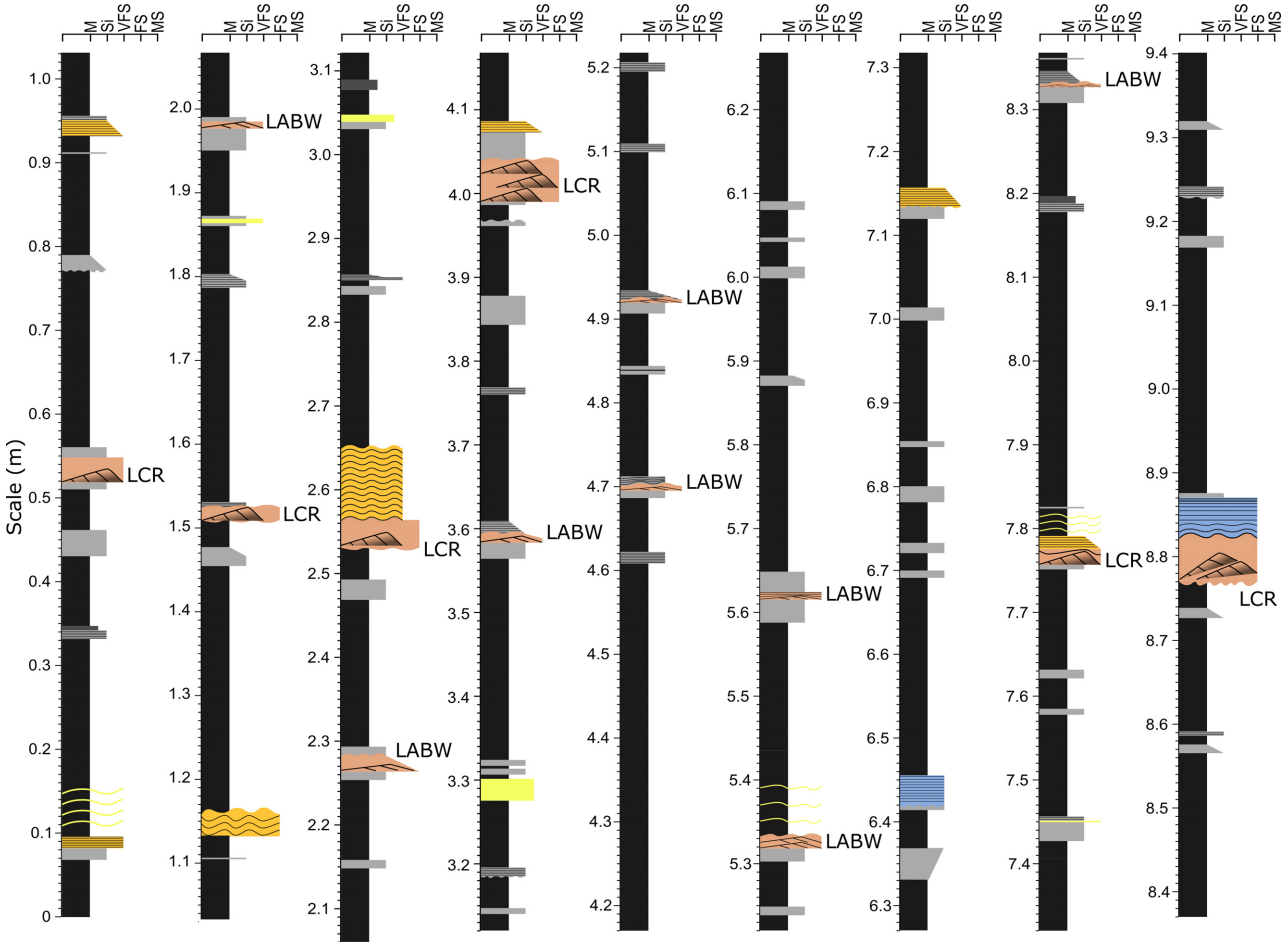

Fig. 7. Sedimentary log D. Position is shown in Fig. 1. LABW, low-amplitude bed-waves; LCR, large current ripples. Scale is in metres.

turbulence-enhanced transitional flows and lower transitional plug flows of Baas *et al.* (2016). The muddy and silty bedform trough fills, basal sections and drapes are attributed to fine particles settling out of suspension during and after flow. To produce the muddy and silty basal division, the bedforms are inferred to have migrated across muds and silts that settled continuously in the troughs of these bedforms (Baas *et al.*, 2016). The fine-grained trough fills of the bedforms resemble sediment-starved ripple profiles, suggesting that the bedform troughs were passively filled with mud or silt during the final phase of bedform migration and after the ripples stopped moving altogether. This was likely associated with a progressive decrease in flow velocity to below the threshold of sediment motion. The presence of the fine-grained drapes confirms that mud kept settling out of suspension after the ripples had stopped moving.

The low-amplitude bed-waves are interpreted to have been formed under lower transitional plug flows and upper transitional plug flows that contained varying proportions of sand and mud. In the laboratory, these flows have a high yield strength and reduced turbulence at the base, which limits the bedforms to long, thin shapes with angles of cross-lamination similar to those in the AGG and BMF (Baas *et al.*, 2016). The low-angle cross-lamination forms as the gently inclined lee side of the bedforms migrates in the flow direction. Fine-grained sediment settling from suspension in the trough of the migrating bedforms is interpreted to generate the climbing muddy basal surfaces.

Heterolithic sandstone–mudstone

Observations

The heterolithic sandstone–mudstone facies is characterized by alternating bands and laminae

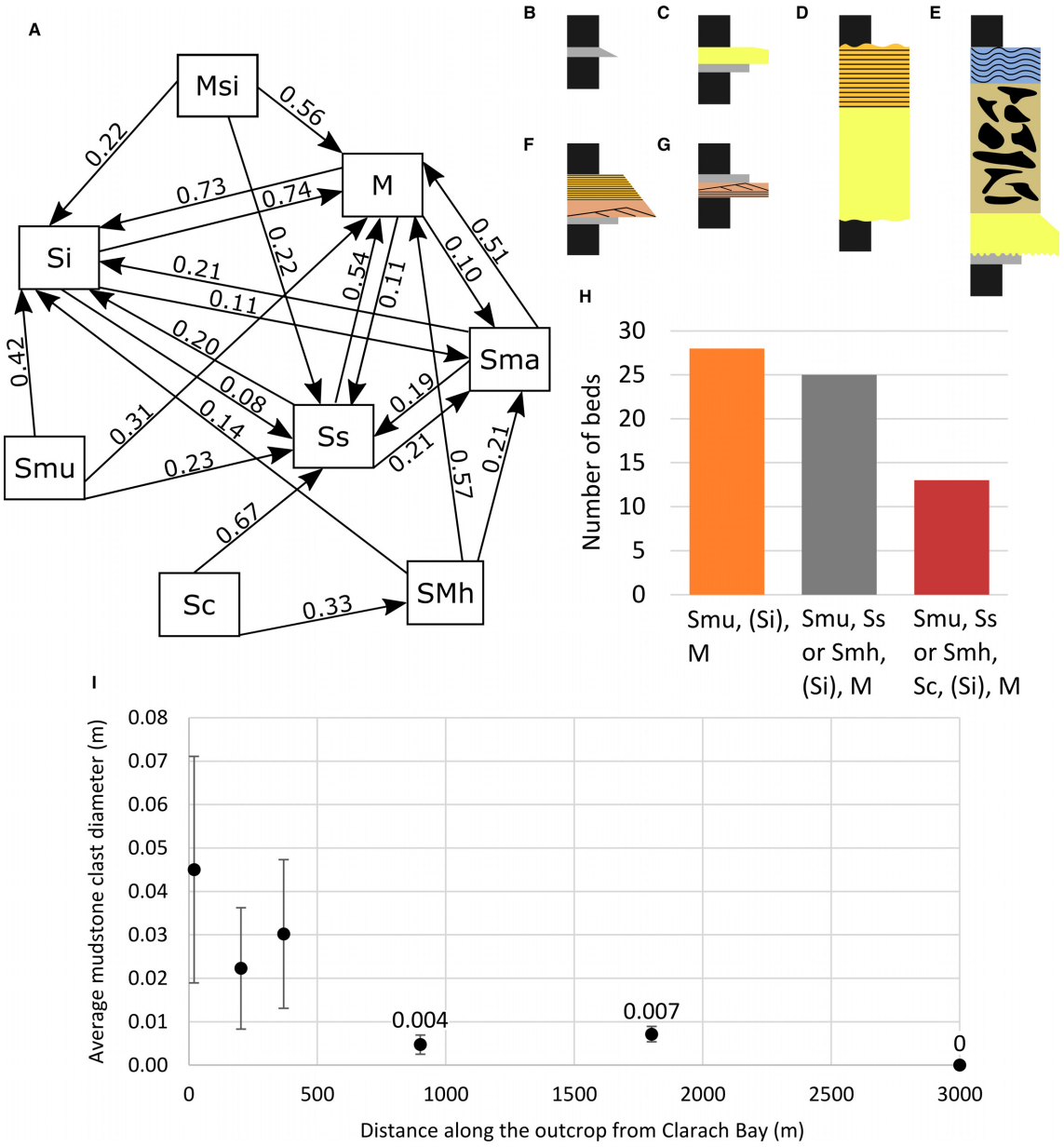

Fig. 8. Results from the Markov chain analysis. (A) Transition tree showing the three most common vertical facies transitions for each facies type with the probability values. M, mudstone; Msi, silty mudstone; Si, siltstone; Sma, massive sandstone; SMh, heterolithic sandstone–mudstone; Smu, structured muddy sandstone; Sc, clast-rich sandstone; Ss, structured sandstone. (B) to (G) show the facies associations identified from the transition tree: (B) fine-grained, thin-bedded turbidites and transitional flow deposits, Facies Association 1 (FA1); (C) thin-bedded turbidites, Facies Association 2 (FA2); (D) medium-bedded turbidites, Facies Association 3 (FA3); (E) clast-rich hybrid event beds, Facies Association 4 (FA4); and (F) and (G) transitional flow deposits, Facies Association 5 (FA5). (H) Plot of the three common vertical facies transitions that include the structured muddy sandstone facies, based on logs and photographs. All structured muddy sandstone beds are above either a mudstone or siltstone. Siltstone at the top of the event beds is not always present and thus shown in brackets. The most common transition is from structured muddy sandstone directly to mudstone, or to mudstone via siltstone (in orange), which corresponds to FA5, shown in (G). The second most likely transition is structured muddy sandstone to either structured sandstone or heterolithic sandstone–mudstone to either mudstone, or siltstone to mudstone (in grey), which corresponds to FA5, shown in (F). The final 20% of the structured muddy sandstone facies were in the following sequence: structured muddy sandstone – heterolithic sandstone–mudstone or structured sandstone – clast-rich sandstone – siltstone – mudstone, or directly from clast-rich sandstone to mudstone (in red). (I) Plot demonstrating that the average mudstone clast diameter decreases with distance along the outcrop from Clarach Bay to Borth.

of light blue–grey, very fine-grained to fine-grained sandstone and black mudstone, in which individual bands are up to 4 mm thick (Fig. 2E). The bands and laminae are plane-parallel or wavy (for example, at 2.15 m and 4.87 m in Fig. 6). Most commonly, the thickness of the mudstone bands increases and the thickness of the sandstone bands decreases upward in the beds. The heterolithic sandstone–mudstone facies has flat and either sharp or diffuse bases, and mostly flat and sharp tops. The bed tops occasionally fine upward.

Interpretation

The origin of the heterolithic character of the heterolithic sandstone–mudstone is unclear. Previous explanations include: (i) phases of waxing and waning of mixed sand–mud gravity flows, where sand and mud are deposited at high and low velocity, respectively (Kneller, 1995); (ii) alternation of deposition of sand by dilute turbidity currents and suspension settling of hemipelagic mud; (iii) rapidly decelerated and highly depositional transitional sand–mud gravity flows of constant velocity, involving cannibalisation of bed material shortly after deposition as a result of reinstated turbulence at decreased flow density (Baas *et al.*, 2016); (iv) a combination of slowly migrating, sandy low-amplitude bedwaves (Best & Bridge, 1992) and continuous suspension settling of fine sediment (Baas *et al.*, 2016); and (v) slurry flows that experience near-bed shear sorting (Lowe & Guy, 2000). The upward increase in mudstone band thickness may indicate an increase in mud content within the flow and a gradual temporal decrease in flow velocity.

Siltstone

Observations

The siltstone facies is composed of dark blue–grey siltstone, often structureless, but also with plane-parallel lamination (for example, at 0.97 m and 1.41 m in Fig. 4; Fig. 2F). Individual laminae are less than 3 mm thick. Beds in the siltstone facies are normally graded, producing gradual tops, or ungraded, with sharp tops. Almost all bed boundaries are flat and the bases of the beds are always sharp.

Interpretation

The siltstone facies were formed by fine-grained, fully turbulent sediment gravity flows or lower transitional plug flows (Baas *et al.*, 2011), from which silt settled out of suspension. The plane-parallel lamination suggests the presence of tractional forces (Piper *et al.*, 1984; Talling *et al.*, 2012).

Silty mudstone

Observations

The silty mudstone facies consists of very dark grey, structureless mudstone with dispersed silt particles, marking it as an intermediate between the siltstone and mudstone facies (Fig. 2G). Slight variations in colour show variations in silt content. Bed bases and tops are sharp and flat (for example, at 8.6 m in Fig. 6).

Interpretation

The silty mudstone facies is interpreted to have formed by fine-grained sediment gravity flows, in which silt particles were not segregated from clay particles during deposition. This suggests that the flows were sufficiently cohesive to prevent vertical segregation of silt and clay. In the laboratory, these flows included upper transitional plug flows and quasi-laminar plug flows (Baas *et al.*, 2011).

Mudstone

Observations

The mudstone facies comprises black uniform mudstone without primary current lamination (Figs 2F and 4 to 7). Bed bases and tops are usually flat and sharp, with a few examples of wavy tops and bases. Slight variations in colour in the form of swirly textures are associated with variations in silt content in thick mudstone facies directly above silty and sandy event beds.

Interpretation

The mudstone facies was generated by hemipelagic settling between events or from the fine-grained components of sediment gravity flows (Bouma, 1962; Talling *et al.*, 2012). The swirly textures are interpreted to have been contained within the plug region of mud-rich, turbulence-attenuated gravity flows, undergoing *en masse* deposition (Baas *et al.*, 2011; Stevenson *et al.*, 2014, fig. 16).

FACIES ASSOCIATIONS

A total number of 777 vertical transitions between the different facies in the sedimentary

logs (Figs 4 to 7) were analysed using Markov chain analysis. The observed counts and probabilities of the vertical transitions are given in Table 1, and the facies relationship diagram in Fig. 8A shows the three most common vertical facies transitions for each facies type. The outcomes of the Markov chain analysis in combination with multi-step facies transitions in the logs were used to construct common facies associations, which were then interpreted in terms of temporal changes in flow behaviour. It was assumed that the mudstone facies separates event beds.

Facies Association 1 (FA1): Fine-grained, thin-bedded turbidites and transitional flow deposits (Fig. 8B)

The Markov chain analysis highlights that the mudstone facies is most commonly overlain by the siltstone facies (probability, $P = 0.73$), and that siltstone is most frequently overlain by mudstone ($P = 0.74$). These isolated siltstone beds, which are common in all of the logs (Figs 4 to 7), are always thin-bedded (<0.05 m) and are interpreted to have been deposited by suspension settling from fine-grained turbidity currents. The presence of swirly textures in the mudstone facies overlying the siltstone facies, observed at Borth, suggests that the flows may have been cohesive; in these cases, FA1 could represent transitional flow deposits.

Facies Association 2 (FA2): Thin-bedded turbidites (Fig. 8C)

This facies association is mainly composed of massive sandstone or structured sandstone encased within mudstone (for example, at 6.19 m in Fig. 5), or siltstone which then transitions upward or downward to mudstone (for example, at 1.81 m in Fig. 6). The upward transitions from massive and structured sandstone to mudstone have the highest probabilities ($P = 0.51$ and $P = 0.54$, respectively). This facies association also includes isolated heterolithic sandstone–mudstone encased in mudstone (for example, at 1.04 m in Fig. 5). FA2 with the massive and structured sandstone is interpreted as the product of sandy turbidity currents. FA2 with heterolithic sandstone–mudstone may have involved turbulent flow or transient turbulent–laminar flow behaviour. FA2 is the facies association most appropriate for the interpretation that heterolithic sandstone–mudstone facies is formed by alternating deposition of sand from dilute turbidity currents and suspension settling of hemipelagic mud.

Facies Association 3 (FA3): Medium-bedded turbidites (Fig. 8D)

Facies Association 3 is made up of thin-bedded to medium-bedded (0.05 to 0.30 m) structured sandstone, massive sandstone and heterolithic sandstone–mudstone, as well as siltstone and mudstone facies. These facies are most commonly organized in partial Bouma sequences denoting waning turbidity currents (Bouma, 1962) and in sequences that represent waxing turbidity currents (*cf.*, Kneller & Buckee, 2000). Examples of this facies association are present in log A at 2.06 m, log B at 0.02 m, and log C at 1.81 m (Figs 4 to 6). FA3 is interpreted as the depositional product of high-density turbidity currents if massive sandstone is the lowermost division. In the absence of massive sandstone, FA3 represents the deposits of low-density turbidity currents. The heterolithic sandstone–mudstone facies is mainly present near the top of FA3 and might therefore represent the T_d-division formed when the flow had waned and possibly attained transitional behaviour.

Facies Association 4 (FA4): Clast-rich hybrid event beds (Fig. 8E)

The clast-rich sandstone facies is interpreted as an upper transitional plug flow or debris-flow deposit and it forms the central division of FA4 (for example, at 6.41 m in Fig. 5). In FA4, clast-rich sandstone is typically underlain by massive sandstone, and overlain by either structured sandstone ($P = 0.67$) or heterolithic sandstone–mudstone ($P = 0.33$). These vertical sequences of facies resemble the products of hybrid flows *sensu* Haughton *et al.* (2009) and Baas *et al.* (2011), where the same event exhibits both laminar and turbulent flow behaviour. Here, a debris flow followed a forerunner high-density turbidity current or transient turbulent flow, and the tail of the event consisted of a low-density turbidity current (structured sandstone) or a transitional plug flow (heterolithic sandstone–mudstone).

Facies Association 5 (FA5): Transitional flow deposits (Fig. 8F and G)

Facies Association 5 includes a variety of distinctive facies successions that include the structured

muddy sandstone facies, which was interpreted to be formed by flows with transient turbulent–laminar behaviour. These facies successions are therefore called transitional flow deposits *sensu* Kane & Pontén (2012). Examples of this facies association are present in log B at 2.94 m, log C at 6.42 m and log D at 8.77 m (Figs 5 to 7).

Of the 25 upward transitions to structured muddy sandstone in the logs, 14 are from siltstone and ten are from mudstone, suggesting that the structured muddy sandstone facies are often near, or at, the base of an event bed. The structured muddy sandstone beds are overlain directly by mudstone (P = 0.31) or by the following facies in order of decreasing P values: siltstone (P = 0.41), structured sandstone (P = 0.23) and heterolithic sandstone–mudstone (P = 0.04).

The structured muddy sandstone facies is the primary facies of interest in this study. Therefore, additional analysis was undertaken using a combination of logs and photographs to investigate the most common sequences of vertical facies transitions that include the structured muddy sandstone beds (Fig. 8H). These sequences were all bounded by mudstone or siltstone. At 42% probability, a single structured muddy sandstone facies between the fine-grained facies was most common (for example, at 5.98 m in Fig. 6). A quarter of the structured muddy sandstone beds transitioned to structured sandstone or heterolithic sandstone–mudstone (for example, at 6.43 m in Fig. 6). The final sequence, with a probability of 20%, was structured muddy sandstone to clast-rich sandstone, via either heterolithic sandstone–mudstone or structured sandstone.

SAND–MUD SEDIMENTARY STRUCTURES

The sedimentary logs, as well as other outcrops in the study area, revealed bedforms in mixed sandstone–mudstone that have not been described in detail in outcrop and core before (*cf.* Figs 9 to 14). The large current ripples (Figs 11 and 12) and low-amplitude bed-waves (Figs 13 and 14) in the structured muddy sandstone of FA5 stand out as having shapes, dimensions, and textural and structural properties that are different from the 'classical' sandy current ripples in the structured sandstone of FA2 and FA3 (Figs 9 and 10). Figure 15 shows the average height and length of the sandy current ripples, the large current ripples and the low-amplitude bed-waves. The diagnostic properties of each bedform type are described below.

Sandy current ripples

The sandy current ripples in the structured sandstone facies in the study area have an asymmetrical shape with a steep lee slope angle of up to 30° and a gentle, longer, stoss slope angle. These bedforms contain high-angle cross-lamination with little variation in grain size (Figs 9 and 10). The sandy current ripples are between 4 mm and 19 mm high (average height, H = 11 mm; standard deviation, σ = 3 mm) and between 89 mm and 216 mm long (average length, L = 141 mm; σ = 31 mm; Fig. 15). These heights and lengths are within the range of current ripples defined by Baas (1999, 2003). The aspect ratio, defined as the bedform height divided by bedform length, of the sandy current ripples ranges from *ca* 0.05 to *ca* 0.15 (Fig. 15).

Large current ripples

The large current ripples in the structured muddy sandstone facies have heights ranging from 13 to 31 mm (H = 19 mm; σ = 4 mm) and lengths ranging from 145 to 433 mm

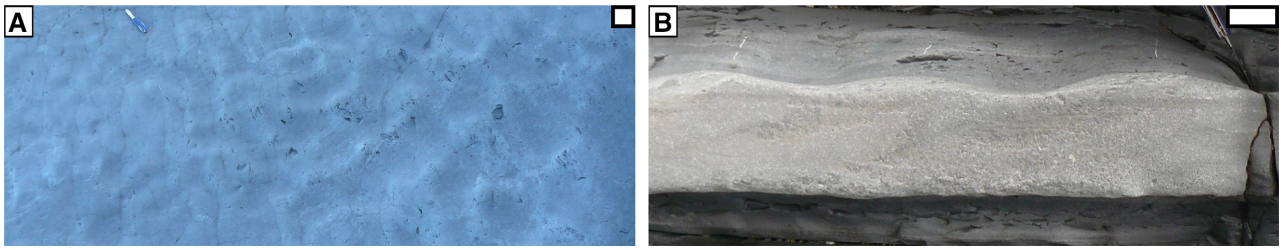

Fig. 9. Examples of sandy current ripples in the field. (A) Ripples in bedding plane, predominantly with a three-dimensional plan form, but with some linearity of the crests in the bottom right of the photograph. (B) Sand-dominated ripples with angle of repose cross-lamination. Scale bar is 50 mm long.

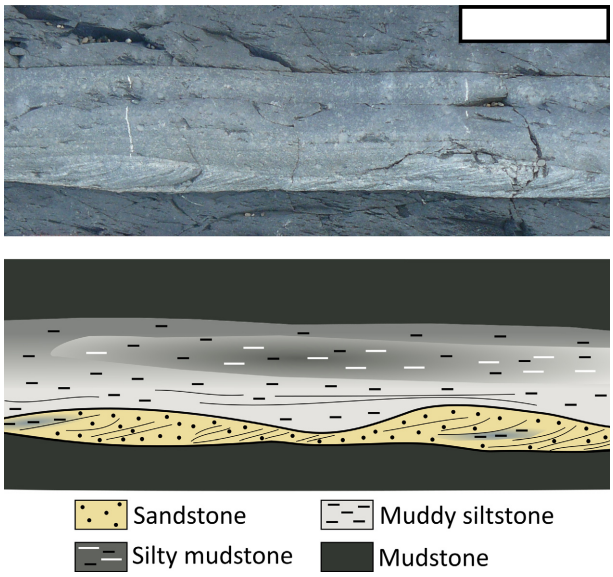

Fig. 10. Picture and schematic drawing of sandstone-dominated sandy current ripples. Note the high-angle cross-lamination. Scale bar is 50 mm long.

(L = 274 mm, σ = 60 mm). The dimensions of the large current ripples are significantly greater than those of the sandy current ripples in the field area, but these bedforms cover a similar range of aspect ratios (Fig. 15). The large current ripples have a variety of forms and textural and structural properties. Many large current ripples have a muddy or silty trough fill, which coarsens to sand in an upstream direction within the bedform (Fig. 11B). Muddy and silty bases that coarsen vertically upward to sand within the bedform are also common (for example, Figs 11A and 12). Some large current ripples had loaded into mud below (Fig. 11C). Thin mudstone layers commonly drape the surface of the large current ripples. These mud drapes tend to extend into the bedform trough and therewith contribute to the trough fill (Fig. 12). Many large current ripples in the field area are climbing bedforms (Fig. 11A and B) with clear high-angle cross-lamination (Fig. 12) and occasional plane-parallel lamination at the base or top of the co-sets (Fig. 11A). Some of the lamination consists of alternating sandstone and mudstone (Fig. 12). When observed on the bedding plane, the large current ripples have pronounced sharp high crests and nearly linear, two-dimensional crest lines (Fig. 11D).

Low-amplitude bed-waves

The low-amplitude bed-waves (LABWs) are bedforms with unusually long lengths of 140 to 818 mm (L = 354 mm, σ = 92 mm) and relatively short heights of 4 to 16 mm (H = 10 mm, σ = 3 mm) (Fig. 15). At 0.0125 to 0.05, the LABWs have lower aspect ratios than the vast majority of the sandy current ripples and the large current ripples (Fig. 15). These bedforms resemble the bed-waves in sand identified under upper-stage plane bed flow conditions by Bridge & Best (1988), who defined the term LABW, and

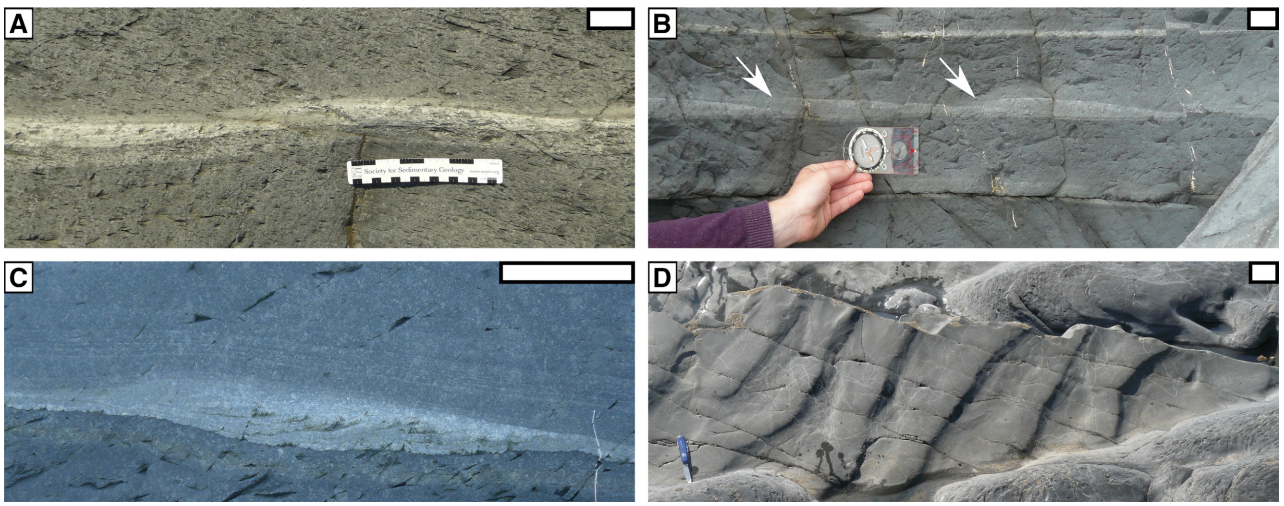

Fig. 11. Examples of large current ripples in the field. (A) Climbing bedforms with a muddy base. (B) Climbing bedforms with muddy trough fills shown by the arrows. (C) Large current ripple loaded into the bed below. (D) In the bedding plane, large current ripples show prounounced, almost linear, two-dimensional crest lines. Scale bar is 50 mm long.

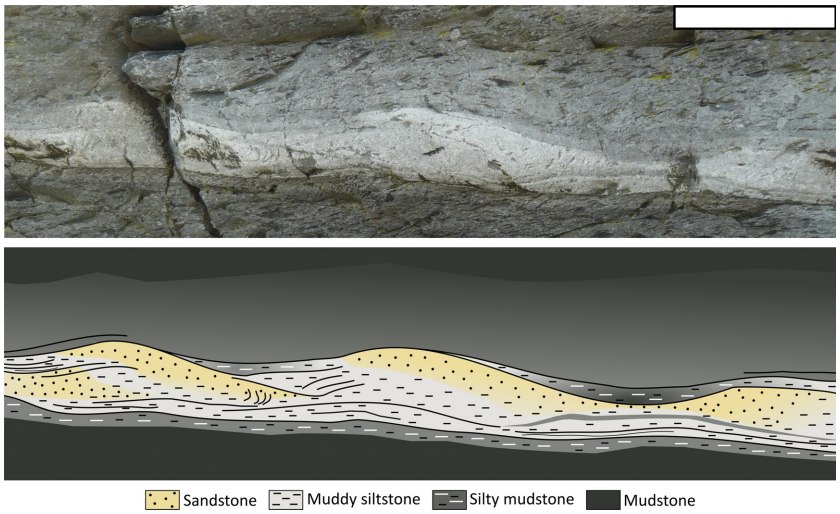

Fig. 12. Schematic drawing of large current ripples with muddy bases and trough fills that coarsen upward and upstream to sandstone. Bedforms contain high-angle cross-lamination, occasionally of alternating sandstone and mudstone. Scale bar is 50 mm long.

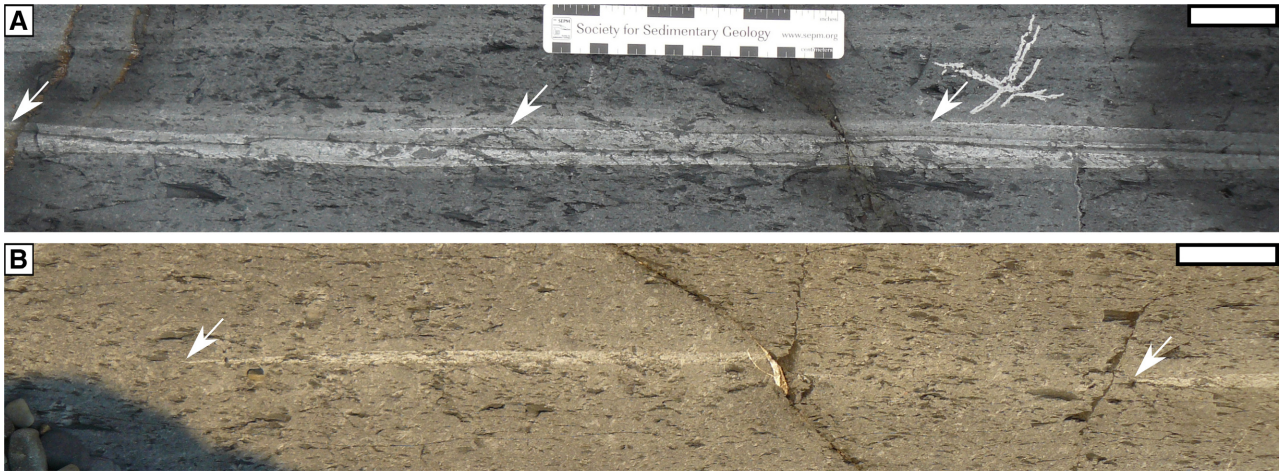

Fig. 13. Examples of low-amplitude bed-waves (LABWs) in the field. (A) Climbing, mixed sandstone–mudstone LABWs with muddy trough fills; arrows point to LABW crests. (B) Lenticular-shaped, sandstone-dominated LABWs isolated in mudstone; arrows point to the preserved lee side of bedforms. Scale bar is 50 mm long.

similar bedforms generated under a range of flow velocities and flow yield strengths in the experiments of Baas *et al.* (2016). The LABWs in the field area are composed of clean sandstone, or, more commonly, mixed sandstone–mudstone. The mixed sandstone–mudstone LABWs often have muddy or silty trough fills and bases which coarsen upward and upstream to sandstone; this can render the lee side of the bedforms hard to distinguish (Figs 13A and 14). These fine-grained bases and trough fills are particularly clear in climbing LABWs, whose climbing surfaces are therefore mudstone-rich (Figs 13A and 14). The sandy LABWs are frequently isolated within mudstone, giving the bedforms a lenticular appearance (Fig. 13B). Internally, the LABWs contain low-angle cross-lamination of *ca* 12° and infrequently plane-parallel lamination near the upflow end of the bedforms (Fig. 14). In the mixed sandstone–mudstone LABWs, these stratification types consist of alternations of sandstone and mudstone (Fig. 14).

Process interpretation of the bedforms

The laboratory experiments of Baas *et al.* (2011, 2016) demonstrated that flows carrying sand, silt and clay change from turbulent via transitional (*sensu* Baas *et al.*, 2009) to laminar as the proportion of cohesive clay is increased. The transitional flows produced different types of bedform and primary current stratification that were

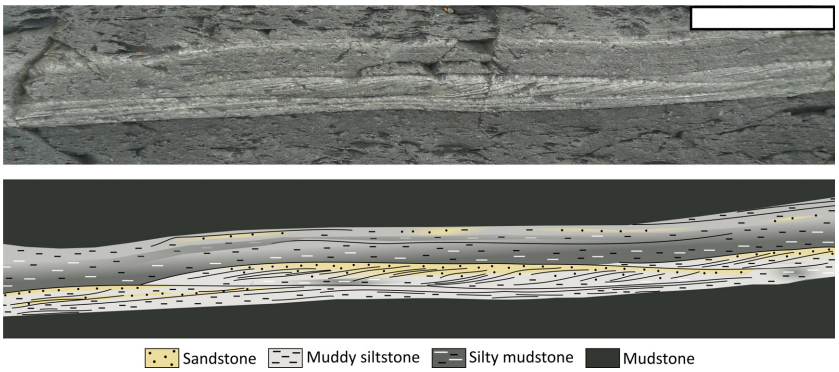

Fig. 14. Schematic drawing of climbing, mixed sandstone–mudstone low-amplitude bed-waves with low-angle cross-lamination and muddy bases and trough fills that coarsen upward and upstream to sandstone. Scale bar is 50 mm long.

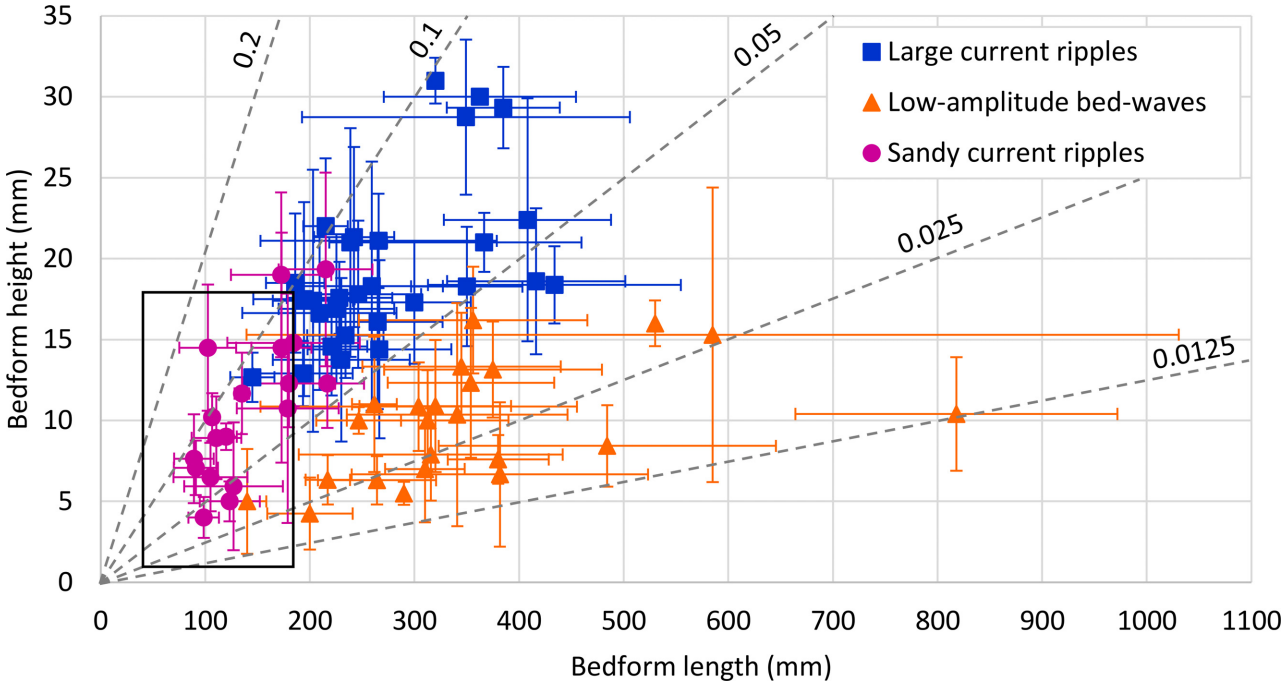

Fig. 15. Height and length of the different bedform types throughout the field area. Dashed lines and associated values show the aspect ratios that characterize the different bedform types. The black box covers the equilibrium and non-equilibrium clear water ripples over the entire grain-size range in which ripples are stable, predicted by Baas (1993).

delimited in a bedform phase diagram based on the cohesive forces in the flow (via the yield strength) and the turbulent forces [via a grain-related mobility parameter, defined by Baas *et al.* (2016) in equation 3]. The present authors propose that the balance between these forces also controls the properties of natural sediment gravity flows and their deposits, and that the bedform phase diagram can therefore be used to interpret the mixed sandstone–mudstone bedforms in the AGG and BMF. Figure 16 shows a schematic summary of the bedform phase diagram of Baas *et al.* (2016).

Sandy current ripples were produced in the laboratory under mixed sand–mud flows with low yield strength (≤0.03 Pa) and grain-related mobility parameters of up to 1.1 (turbulent flow of Baas *et al.*, 2016; Fig. 16). The low yield strength of these flows implies that the turbulent fluctuations in flow velocity were strong enough to prevent the clay minerals from forming bonds. The dynamics of these flows were therefore interpreted to be similar to clear water flows, where the frictional forces between the flow and substrate shaped the bed into 'classical' current ripples, which are typically <20 mm

high and <200 mm long, with aspect ratios <0.1 (Baas, 2003). The average height of 11 mm, average length of 141 mm and mean aspect ratio of 0.076 of the sandy current ripples in the AGG are within this range. These ripples are therefore interpreted to have formed under fully turbulent conditions, i.e. by turbulent sandy gravity flows (equivalent to turbulent flow of Baas *et al.*, 2016; Fig. 16).

Another type of current ripple produced in the laboratory by decelerated mixed sand–mud flows was characterized by heights and lengths that were greater than the dimensions of sandy current ripples (Baas *et al.*, 2011). These so-called large ripples contained sand, silt and clay that were distributed differently within the bedform as a function of ripple development stage. Initially, the bedforms had a muddy core below cross-laminated sand, which then developed into cross-laminae consisting of alternating mud and sand, and finally into mixed sand–mud cross-laminae (Baas *et al.*, 2011, fig. 14).

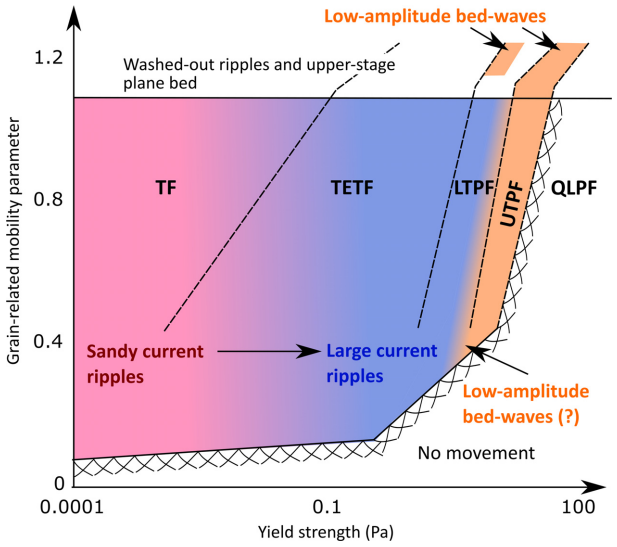

Fig. 16. Schematic summary of the bedform phase diagram of Baas *et al.* (2016) for rapidly decelerated mixed sand–mud flows, based on grain-related mobility parameter and yield strength of the suspension. The colours represent the stability fields of the three bedform types observed in this study. The dashed lines represent the boundaries between the different flow types. Note that this diagram is based on a limited range of boundary conditions; in particular, the field boundaries of the low-amplitude bed-waves are approximate at present. LTPF, lower transitional plug flow; TF, turbulent flow; TETF, turbulence-enhanced transitional flow; UTPF, upper transitional plug flow; QLPF, quasi-laminar plug flow.

The bedforms classified as large current ripples in the study area are comparable to the large current ripples of Baas *et al.* (2011) in their mixed sand–mud composition, large size, muddy base and alternating sand–mud cross-laminae. In the laboratory, the large current ripples formed under the same range of mobility parameters as the sandy current ripples, but the flows had greater yield strengths (0.03 to 3 Pa; Fig. 16). These flows were classed as turbulence-enhanced transitional flows and lower transitional plug flows (Baas *et al.*, 2016), in which near-bed turbulence was enhanced because the cohesive strength of the flows promoted the development of an internal shear layer. This increased turbulence caused stronger erosion in the lee of the bedforms, thus increasing their height and length compared to sandy current ripples (Baas *et al.*, 2011). It is therefore inferred that the large current ripples in the AGG and the BMF were formed by sediment gravity flows with turbulence-enhanced transitional flow and lower transitional plug flow behaviour. The fact that the large ripples observed in the field area were dominated by muddy bases and alternating sandstone–mudstone cross-laminae suggests that these bedforms were in a relatively early stage of development, as in the experiments of Baas *et al.* (2011). This agrees with the generally short migration distance of the climbing large ripples (for example, Fig. 12), which is typical of rapidly decelerated and highly depositional sediment gravity flows.

The laboratory experiments of Baas *et al.* (2016) also produced long, thin bedforms — low-amplitude bed-waves (LABWs) — with heights of 3 to 16 mm and lengths of 70 to 5000 mm (Baas *et al.*, 2016, figs 19 and 20A). These bedforms consisted of sand or mixed sand–mud, where the sand and mud were either uniformly mixed or heterolithic. Low-angle cross-lamination in the LABWs was often composed of alternating laminae of sand and mud. The lowest 20 to 30% of the mixed sand–mud LABWs was usually rich in mud. These properties are analogous to those observed in the field. Although also found in lower transitional plug flow, the experimental LABWs were most typically produced by upper transitional plug flows at a wide range of mobility parameters, covering flows that would form upper-stage plane bed, washed-out ripples and sandy current ripples in clay-poor turbulent flow (Baas *et al.*, 2016; Fig. 16). These LABWs formed at yield strengths between *ca* 1 to 4 Pa in plug flows with

attenuated turbulence at the base (Baas *et al.*, 2009). The authors infer that the LABWs in the AGG and BMF were formed under similar flow conditions.

Spatial distribution of the bedforms in the field area

Figure 17 shows the spatial distribution of the sandy current ripples, large current ripples and LABWs throughout the study area, subdivided into four sections of the coastal outcrops from the fringe to the distal fringe of the fan. In the most proximal part of the study area, between Aberystwyth and Clarach Bay, sandy current ripples are the most common bedform type, followed by LABWs, with only a few examples of large current ripples (Fig. 17). Moving north and more distally, the number of sandy current ripples decreases, and no sandy current ripples are present at Borth. Large current ripples are the most common bedform type in the two central sections of the study area, although LABWs are also widespread (Fig. 17). At Borth, LABWs account for the largest proportion of bedform types, with subordinate occurrences of large current ripples.

DISCUSSION

Using bedforms to infer flow processes in the fringe region of the Aberystwyth Grits Group and Borth Mudstone Formation

Baas *et al.* (2016) showed that flow type and bedform type are closely linked. In the laboratory, increasing clay concentration caused turbulence modulation and changed turbulent flow via transitional flow to laminar flow, which in turn produced sandy current ripples, large current ripples and LABWs (Fig. 16). In the AGG and BMF, the dominant bedform type changed from sandy current ripples via large current ripples to LABWs from the fringe of the system near Aberystwyth to the distal fringe of the system at Borth. However, it is important to note that for each of the four sections of outcrop an assemblage of bedforms was observed, which attests to a variety of flow types reaching individual locations. The observed change in the prevailing bedform type from Aberystwyth to Borth indicates that many of the flows transformed from turbulent flow, via turbulence-enhanced transitional flow and lower transitional plug flow, to upper transitional plug flow as they travelled through the fringe to the distal fringe of the fan (Fig. 18).

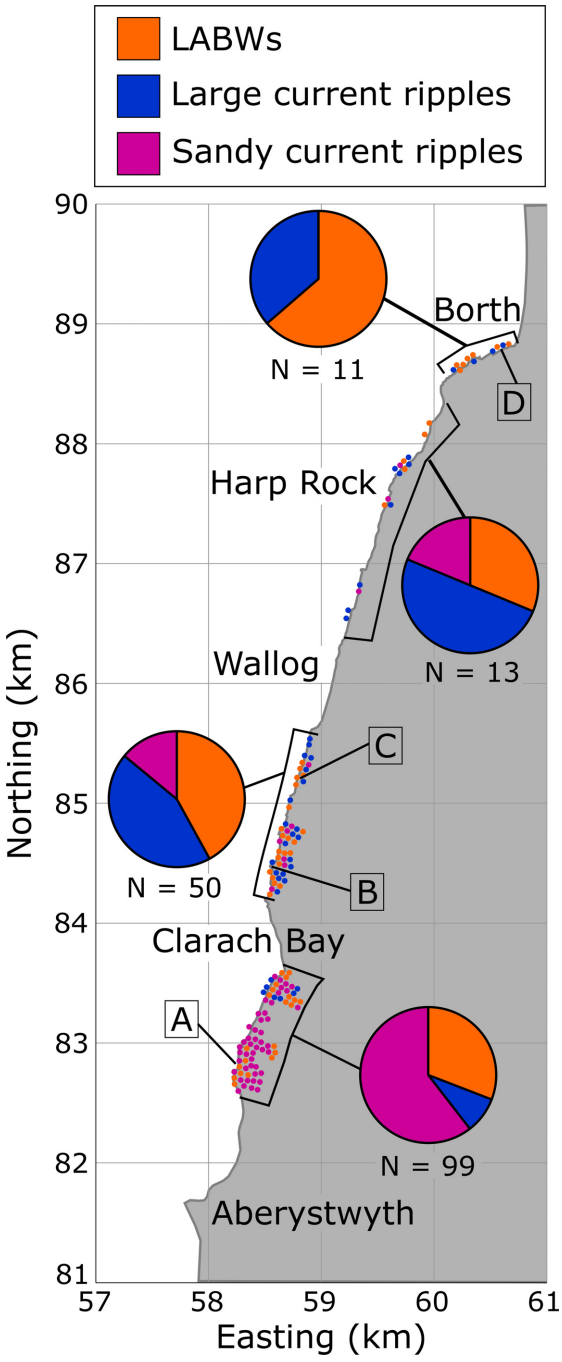

Fig. 17. Spatial distribution of the bedforms in the field area. Each dot represents a bedform observation. Pie charts show the proportion of bedform types for each section of accessible outcrop. Letters 'A' to 'D' show locations of the logs. *N* = number of bedforms for the pie chart. LABWs, low-amplitude bed-waves.

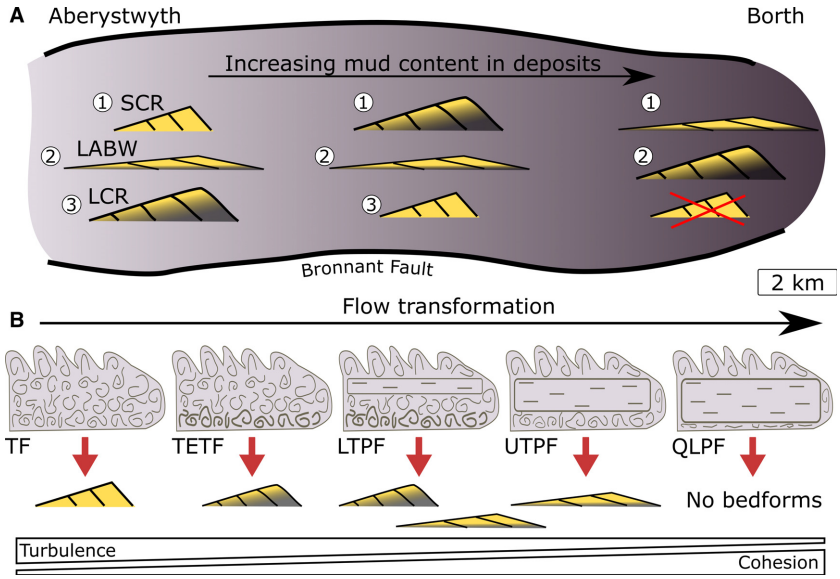

Fig. 18. (A) Schematic plan view of the fringe to distal fringe of the fan in the Aberystwyth Grits Group and the Borth Mudstone Formation, confined within an elongate sub-basin of the Welsh Basin, with the different bedform assemblages found throughout the studied part of the fan. Numbers in (A) denote observed bedform type in order of decreasing frequency. LABW, low-amplitude bed-waves; LCR, large current ripples; SCR, sandy current ripples. (B) Model of flow transformation from the fringe to the distal fringe of the fan, and the link between sediment gravity flow dynamics and the bedforms produced. TF, turbulent flow; TETF, turbulence-enhanced transitional flow; LTPF, lower transitional plug flow; UTPF, upper transitional plug flow; QLPF, quasi-laminar plug flow.

Flow transformation has been shown to be key in interpreting spatial trends in deposit type in the fringe of other deep-marine systems, such as Late Jurassic fans in the northern North Sea (Haughton *et al.*, 2003) and in the Tanqua Karoo system (Kane *et al.*, 2017). Flow transformation occurs when flows react to changing boundary conditions. Consequently, the flow may alter its velocity, deposit or erode sediment, incorporate water and increase the flow height, or dewater and reduce the flow height. The Reynolds number, *Re*, can be used to describe flow behaviour and transformation, representing the ratio of inertial and viscous forces:

$$Re = \frac{Uh}{\nu} \quad (1)$$

where U is the depth-averaged current velocity, h is the flow height and ν is the apparent kinematic viscosity. Apparent viscosity is used for non-Newtonian suspensions, such as shear thinning clay-laden flows, where the viscosity parameter changes with shear rate. The *Re* can be used to differentiate flow types: high *Re* values represent fully turbulent flows and low *Re* values characterize laminar flows, with transitional flow behaviour found between these two end members. In the experiments of Baas *et al.* (2009), the boundary between laminar flow and transitional flow was at $Re = 7000$ and the boundary between turbulent flow and transitional flow was at $Re = 55\,000$.

To produce the observed changes in dominant bedform type from Aberystwyth to Borth, the inferred flow transformation from turbulent flow to upper transitional plug flow, via turbulence-enhanced transitional flow and lower transitional plug flow, requires *Re* to decrease from the fringe to the distal fringe of the basin. Below, *Re* is used to interpret which flow parameters in Eq. 1 altered as the flows transformed through the study site and prompted the observed trend in dominant bedform type. In the *Re*-based analysis herein, it is assumed that the sediment gravity flows were predominantly depositional and did not erode sediment from the bed in the studied part of the fan. This is supported by the fact that evidence for scour in the log data and from other observations in the field area is limited to sole marks that are not deeper than a few centimetres. This demonstrates that the flows progressively lost sand and silt, and thus the relative proportion of mud in the flows increased, from the fringe to the distal fringe

of the system. These textural changes are expressed by thickening mudstone facies, decreasing frequency and thinning of massive sandstone and structured sandstone facies, and an increase in the number of structured muddy sandstone and heterolithic sandstone–mudstone facies (Figs 4 to 7). In turn, these facies changes provide further evidence for the inferred transformation from turbulent via transitional to laminar flows, resulting from the decrease in *Re*. In addition, the inferred disaggregation of mud clasts as the flows travelled through the system from Clarach Bay to Borth (Fig. 8I) is another process that could have increased the relative proportion of mud in the flow and promote flow transformation.

The progressive loss of sand and silt between the fringe and the distal fringe of the fan implies that the density difference between the flow and the ambient fluid was reduced, thus leading to the deceleration of the sediment gravity flows. The thick mudstone caps at Borth suggest that large amounts of clay were carried to the fringe of the fan (see *Mudstone cap analysis* below). It is therefore unlikely that the viscosity of the flows decreased as a result of clay deposition along the transport path. Instead, the authors expect the viscosity to have increased because of the shear thinning nature of the clay-rich flows. Shear thinning behaviour enables the viscosity to increase at a constant clay concentration when a reduction in flow velocity, and hence shear rate, enables a network of cohesive bonds between clay particles to develop (Coussot, 1997; Talling, 2013). Equation 1 demonstrates that the deceleration of the cohesive sediment gravity flows between Aberystwyth and Borth, and the increased viscosity due to shear thinning, both contribute to a reduction of *Re*, thus aiding the flow transformation.

The flow height term in *Re* is difficult to interpret from the rock record, because the deposits of only quasi-laminar plug flows, i.e. debris flows, can be related to the original flow thickness (Kneller & Branney, 1995; Talling *et al.*, 2012). However, laboratory experiments have shown that the amount of mixing at the upper boundary of sediment gravity flows decreases as the flow viscosity increases (Marr *et al.*, 2001; Mohrig & Marr, 2003; Baker *et al.*, 2017). Increasing the stability of the upper boundary reduces the ability of the flow to incorporate water. Given the inferred increase in viscosity from the fringe to the distal fringe of the fan, it is therefore unlikely that flow height was able to increase much along this transect. Numerical simulations constrained by field data also suggest that steady-state turbidity currents form stratified flows with a lower layer of consistent flow height containing the majority of the suspended sediment (Kneller *et al.*, 2016; Luchi *et al.*, 2018). A decrease in flow height could have occurred if the flows were able to spread laterally in the distal part of the system following a loss of confinement. The 2D nature of the outcrops does not allow the amount of flow confinement to be verified. However, it is likely that the confined linear shape of the basin (Cherns *et al.*, 2006; Gladstone *et al.*, 2018) limited lateral spreading of the flows and helped maintain the flow height. Finally, the deposition of sand and silt between Aberystwyth and Borth induced by flow deceleration could have decreased the flow thickness (Kneller & Branney, 1995). A constant or decreasing flow height in combination with flow deceleration and increasing flow viscosity, as the flows travelled from the fringe to the distal fringe of the fan, would further reduce *Re*, promote flow transformation and explain the observed trend in dominant bedform type (Fig. 18).

Mudstone cap analysis

Turbiditic and hemipelagic mudstone cannot be visually distinguished from one another in the AGG and BMF (Talling, 2001). However, part of the mudstone facies in the distal fringe of the system around Borth contained slight variations in colour in the form of swirly textures, associated with coherent variations in silt content. These swirly textures are interpreted to have been confined within the plug region of a mud-rich, turbulence-attenuated upper transitional plug flow or quasi-laminar plug flow, which underwent *en masse* deposition enabling the structures to be preserved (e.g. Stevenson *et al.*, 2014). Hemipelagic settling is unlikely to produce these swirly textures. Moreover, the thickness of mudstone facies of hemipelagic origin is not expected to correlate with the thickness of underlying event beds. Instead, it was hypothesized that larger events produce thicker flow-derived mudstone caps. To determine whether an event bed and the mudstone facies above it were indeed formed by the same flow, linear regression analysis was undertaken comparing the thickness of the event beds and the overlying mudstone facies in the four sedimentary logs. The best-fit line between event bed and mudstone cap thickness was forced through the (0,0) intercept.

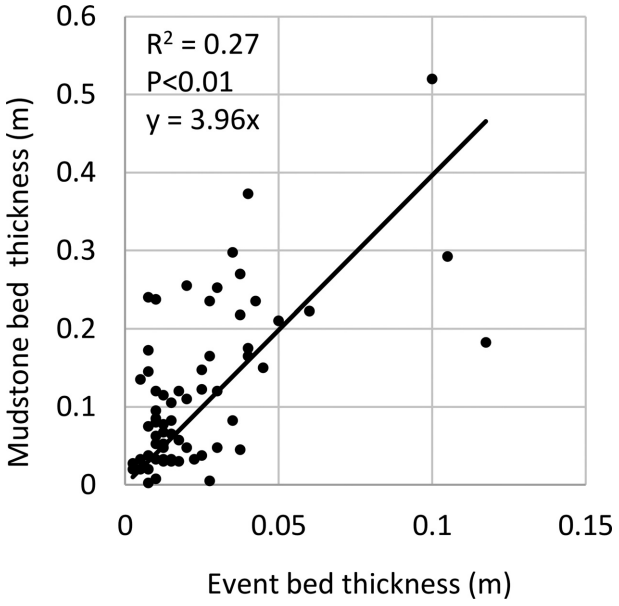

Fig. 19. Event bed thickness and overlying mudstone bed thickness for log D. Black line denotes least-squares linear fit to data.

No statistically significant correlation between event bed thickness and mudstone cap thickness was found for logs A to C. However, for log D located at Borth, these thicknesses correlate positively, with an $R^2 = 0.27$ ($P < 0.01$; Fig. 19). This supports the hypothesis herein that a statistically significant number of the mudstone caps were flow derived. These mudstone caps were partly formed by *en masse* freezing of upper transitional plug flows and quasi-laminar plug flows, which led to the preservation of the swirly silt textures. The lack of correlation between the thickness of the event beds and their mudstone caps in logs A to C is interpreted to result from the mud dominantly bypassing in faster, more turbulent flows. This finding supports the spatial distribution of the bedform types through the system, which was interpreted above to indicate longitudinal flow transformation to increasingly cohesive transitional flows at the distal fringe of the fan at Borth.

Hybrid event beds in the fringe of a mud-rich submarine fan

Figure 8H shows that structured muddy sandstone facies can be part of the following facies sequence: structured muddy sandstone – heterolithic sandstone–mudstone – clast-rich sandstone – siltstone – mudstone, or directly from clast-rich sandstone to mudstone. This sequence resembles the hybrid event bed model of Haughton *et al.* (2009), where: (i) heterolithic sandstone–mudstone is equivalent to the H2 division of banded mud-poor sandstone and mud-rich sandstone, formed by transitional flow; (ii) clast-rich sandstone fits the H3 section of argillaceous sandstone rich in sandstone and mudstone clasts, formed by debris flow; and (iii) siltstone and mudstone resemble the H4 and H5 divisions, formed by low-density turbidity current and mud suspension fallout (*cf.* Fig. 20). The structured muddy sandstone facies at the base of these event beds diverges from the basal H1 division in the model of Haughton *et al.* (2009) by being structured and consisting of mixed sandstone–mudstone instead of comprising massive and structureless sandstone (Fig. 20). In the Haughton *et al.* (2009) model, the H1 division was interpreted to have formed by a non-cohesive, high-density turbidity current. An alternative explanation for the AGG and BMF is proposed below.

Fig. 20. Examples of bedforms within the H1 division of hybrid event beds: (A) Large current ripples, (B) climbing sandy current ripples, and (C) low-amplitude bed-waves with low-angle cross-lamination outlined. Scale bar is 50 mm long.

Table 2. Diagnostic criteria of sandy current ripples, large current ripples and low-amplitude bed-waves to aid identification in the field and in core. Arrows point to cross-lamination of sandy current ripples and the bedform crests of the large current ripples and low-amplitude bed-waves. Scale bar is 50 mm long.

	Sandy current ripples	Large current ripples	Low-amplitude bed-waves
Good photograph example	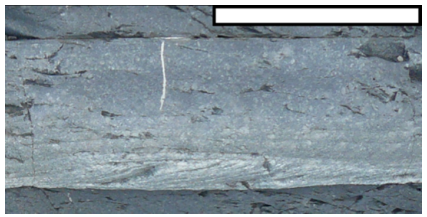	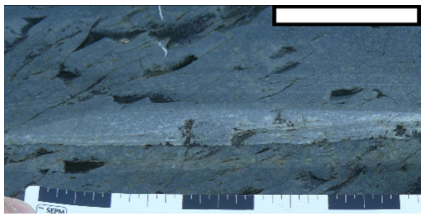	
Poor photograph example	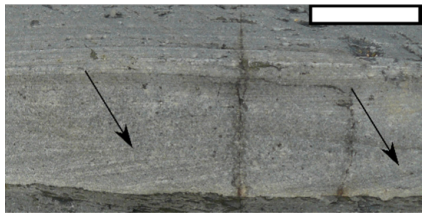		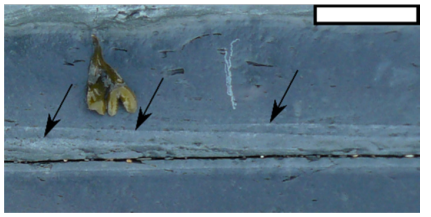
Texture	• Sandstone-dominated • Asymmetrical profile	• Mixed sandstone–mudstone • Asymmetrical profile • Muddy or silty trough fill and/or base that coarsens upstream and/or upward to sandstone • Climbing and non-climbing • Mudstone layers may drape bedform surface	• Mixed sandstone–mudstone or sandstone dominated • Muddy or silty trough fill and/or base that coarsens upstream and/or upward to sandstone • Climbing and non-climbing • Climbing surfaces often mudstone-rich • Bedforms can be isolated in mudstone
Dimensions	• Heights = <20 mm • Lengths = <200 mm	• Heights = *ca* 10–30 mm • Lengths = *ca* 140–430 mm	• Heights = *ca* 4–16 mm • Lengths = *ca* 140–820 mm
Cross-lamination	• High-angle cross-lamination of *ca* 30°	• High-angle cross-lamination of *ca* 30° • Plane-parallel lamination at the base or top of co-sets • Laminae may consist of alternating sandstone–mudstone	• Low-angle cross-lamination of *ca* 12° • Plane-parallel lamination near the upflow end of the bedforms • Laminae may consist of alternating sandstone–mudstone

Hybrid event beds have been defined as deposits produced by flows which transform from poorly cohesive, turbulent to cohesion-dominated (Haughton *et al.*, 2009; Fonnesu *et al.*, 2015; Pierce *et al.*, 2018). Based on the observations in the AGG and BMF, it is proposed here that mud-rich hybrid event beds at the fringe of a system may contain argillaceous H1 divisions with mixed sandstone–mudstone bedforms. The H1 division in these mud-rich hybrid event beds need not be formed by a high-density turbidity current, but could result from transitional flow, in which flow turbulence is modulated by cohesive forces throughout deposition, as also previously suggested by Baas *et al.* (2011). By analogy to the laboratory experiments of Baas *et al.* (2009), these flows could include turbulence-enhanced transitional flow, lower transitional plug flow, and upper transitional plug flow. If hybrid event beds with large current ripples and LABWs in basal mixed sandstone–mudstone are also present in other deep-marine systems, this extended model for the origin of hybrid event beds could help to interpret their formation by including an increased range of turbulence-modulated flow types.

Mixed sand–mud bedforms in other deep-marine systems

The identification of large current ripples and low-amplitude bed-waves, in addition to sandy current ripples, shows that a diverse range of bedforms may be present in the mud-rich outer part of a submarine fan. Since these mixed sand–mud bedforms are formed by transitional to laminar flows, the deposits of which have been shown to be common in many fine-grained submarine fans (e.g. Haughton *et al.*, 2009; Kane & Pontén, 2012; Kane *et al.*, 2017), it is likely that mixed sand–mud bedforms are present in the fringe to the distal fringe of other mud-rich deep-marine systems. It is proposed herein that mixed sand–mud bedforms are valuable as an additional indicator for the outer margins of mud-rich systems, in combination with hybrid event beds, thin sandy turbidites and mud-rich turbidites, thus aiding the interpretation of the deep-marine sedimentary record. These bedforms may also be present in the fringe of more sand-dominated systems, in which deposition has also been shown to be controlled by cohesive clay, for example, the sandy Late Jurassic deep-water fans in the North Sea (Haughton *et al.*, 2003).

The spatial trend in dominant bedform type is attributed to flow transformation from the fringe to the distal fringe of the system, informed by the strong relationship between the flow type and bedform type found in laboratory experiments. Flow transformations have been shown to occur in the fringe of other submarine fans, such as the Ross Formation (Pyles & Jennette, 2009) and the Skoorsteenberg Formation (Kane *et al.*, 2017). Thus, assemblages of sandy current ripples, large current ripples and LABWs could be used as an additional predictive tool to determine a more precise location within the fringe and, particularly, the distal fringe of other deep-marine systems. The results of this study show that the distal fringe of a system may be dominated by turbulence-modulated flows that form large current ripples, and in particular LABWs, whereas more proximal portions of the fringe of the system may show a majority of sandy current ripples formed by fully turbulent flows (Fig. 18).

The exceptional exposure of the AGG and BMF aided the identification of the mixed sandstone–mudstone bedforms based on texture, internal composition, bedform dimensions and style of cross-lamination. It may not be possible in outcrops with poor exposure to determine bedform types based on all of the diagnostic criteria, but bedform size and angle of cross-lamination, using the quantitative data detailed herein, should enable differentiation between sandy current ripples, large current ripples and LABWs. Recognizing LABWs and large current ripples need not be confined to outcrop studies. A powerful aspect of utilising these mixed sand–mud bedforms is that they are small enough to be partly observed in core. Although the full length of large current ripples and LABWs cannot be captured in core, the height of the bedforms and the style of the cross-lamination should enable the interpretation of the mixed sand–mud bedform type. To aid bedform identification in field and core studies, a summary of the diagnostic criteria for the three bedform types is provided in Table 2.

CONCLUSIONS

The identification of novel, mixed sand–mud bedforms in the fringe of the mud-rich deep-marine system of the Aberystwyth Grits Group (AGG) and Borth Mudstone Formation (BMF) suggests that the sedimentary structures in the fringe of fine-grained submarine fans may be

more diverse than previously thought. The strong link between flow type and bedform type in decelerated mixed sand–mud flows, as previously demonstrated in laboratory experiments, allows the sandy current ripples, large current ripples and low-amplitude bed-waves to be used to reconstruct formative flow type in the outer part of submarine fans. Sandy current ripples form under fully turbulent flows, large current ripples are generated under turbulence-enhanced transitional flows and lower transitional plug flows, and low-amplitude bed-waves primarily form under upper transitional plug flows.

The downdip trend of dominant bedform type from sandy current ripples, via large current ripples, to low-amplitude bed-waves suggests that the flows in the study area underwent transformation from turbulent via transitional to laminar on their way to the distal fringe of the fan. This flow transformation can be interpreted as representing a declining flow Reynolds number, mainly caused by flow deceleration following sediment deposition and increasing viscosity related to the shear-thinning nature of the clay-rich suspensions. The strongly cohesive flows at the fringe of the fan produced hybrid event beds with mixed sandstone–mudstone bedforms instead of massive sandstone in the H1 division. This suggests that the hybrid event bed model can be extended to the deposits of mud-rich hybrid events that include H1 divisions formed by cohesive transitional flows, rather than high-density turbidity currents. Moreover, at the fringe of the AGG–BMF system, the positive linear correlation between event bed thickness and the thickness of the overlying mudstone beds suggests that these mudstone caps may have been formed partly from strongly cohesive transitional and laminar sediment gravity flows.

Large current ripples and low-amplitude bed-waves are likely to be present in the fringe of other deep-marine systems. These bedforms may therefore have value as additional indicators for the outer margins of deep-marine systems and can be used to aid prediction of the depositional processes in these sub-environments.

ACKNOWLEDGEMENTS

The authors are grateful to Holly Bargh, Aaron Metcalf, Rebecca Seal and Richard McKee for their help with the data collection in the field. This project was kindly funded by Equinor. We would like to thank reviewers Christopher Stevenson, Esther Sumner and James Best for their detailed and helpful reviews that greatly improved the manuscript.

DATA AVAILABILITY STATEMENT

The data that support the findings of this study are available from the corresponding author upon reasonable request.

REFERENCES

Allen, J.R.L. (1968) *Current Ripples: Their Relation to Patterns of Water and Sediment Motion*. North-Holland Publishing Company, Amsterdam, 433 pp.

Allen, J.R.L. (1971) Instantaneous sediment deposition rates deduced from climbing-ripple cross-lamination. *J. Geol. Soc. London*, **127**, 553–561.

Allen, J.R.L. (1982) *Sedimentary Structures, their Character and Physical Basis*, Volumes **1, 2**. Elsevier, Amsterdam, 593 pp, 663 pp.

Arnott, R.W.C. and **Hand, B.M.** (1989) Bedforms, primary structures and grain fabric in the presence of suspended sediment rain. *SEPM J. Sed. Res.*, **59**, 1062–1069.

Ashley, G.M., **Southard, J.B.** and **Boothroyd, J.C.** (1982) Deposition of climbing-ripple beds: a flume simulation. *Sedimentology*, **29**, 67–79.

Baas, J.H. (1993) Dimensional analysis of current ripples in recent and ancient depositional environments. *Geol. Ultraiect.*, **106**, 199.

Baas, J.H. (1999) An empirical model for the development and equilibrium morphology of current ripples in fine sand. *Sedimentology*, **46**, 123–138.

Baas, J.H. (2003) Ripple, ripple mark, ripple structure. In: *Encyclopedia of Sediments and Sedimentary Rocks* (Ed. Middleton, G.V.), pp. 565–568. Kluwer Academic Publishers, Dordrecht.

Baas, J.H. and **Best, J.** (2002) Turbulence modulation in clay-rich sediment-laden flows and some implications for sediment deposition. *J. Sed. Res.*, **72**, 336–340.

Baas, J.H., **Best, J.L.**, **Peakall, J.** and **Wang, M.** (2009) A phase diagram for turbulent, transitional, and laminar clay suspension flows. *J. Sed. Res.*, **79**, 162–183.

Baas, J.H., **Best, J.L.** and **Peakall, J.** (2011) Depositional processes, bedform development and hybrid bed formation in rapidly decelerated cohesive (mud-sand) sediment flows. *Sedimentology*, **58**, 1953–1987.

Baas, J.H., **Davies, A.G.** and **Malarkey, J.** (2013) Bedform development in mixed sand–mud: the contrasting role of cohesive forces in flow and bed. *Geomorphology*, **182**, 19–32.

Baas, J.H., **Best, J.L.** and **Peakall, J.** (2016) Predicting bedforms and primary current stratification in cohesive mixtures of mud and sand. *J. Geol. Soc.*, **173**, 12–45.

Baker, M.L., **Baas, J.H.**, **Malarkey, J.**, **Jacinto, R.S.**, **Craig, M.J.**, **Kane, I.A.** and **Barker, S.** (2017) The effect of clay type on the properties of cohesive sediment gravity flows and their deposits. *J. Sed. Res.*, **87**, 1176–1195.

Barker, S.P., **Haughton, P.D.W.**, **McCaffrey, W.D.**, **Archer, S.G.** and **Hakes, B.** (2008) Development of rheological heterogeneity in clay-rich high-density turbidity currents:

Aptian Britannia Sandstone Member, U.K. Continental Shelf. *J. Sed. Res.*, **78**, 45–68.

van, den Berg, J.H. and **van, Gelder, A.** (1993) A new bedform stability diagram, with emphasis on the transition of ripples to plane bed in flows over fine sand and silt. In: *Alluvial Sedimentation* (Eds Marzo, M. and Puigdefabregas, C.), Int. Assoc. Sedimentol. Spec. Publ., **17**, 11–21.

Best, J.L. and **Bridge, J.S.** (1992) The morphology and dynamics of low amplitude bedwaves upon upper stage plane beds and the preservation of planar laminae. *Sedimentology*, **39**, 737–752.

Bouma, A.H. (1962) *Sedimentology of Some Flysch Deposits: A Graphic Approach to Facies Interpretation*. Elsevier, Amsterdam, 168 pp.

Bridge, J.S. and **Best, J.L.** (1988) Flow, sediment transport and bedform dynamics over the transition from dunes to upper-stage plane beds: implications for the formation of planar laminae. *Sedimentology*, **35**, 753–763.

Cherns, L., **Cocks, L.R.M.**, **Davies, J.R.**, **Hillier, R.D.**, **Waters, R.A.** and **Williams, M.** (2006) Silurian: the influence of extensional tectonics and sea-level changes on sedimentation in the Welsh Basin and on the Midland Platform. In: *The Geology of England and Wales* (Eds Brenchley, P.J. and Rawson, P.F.), pp. 75–102. The Geological Society, London.

Coussot, P. (1997) *Mudflow Rheology and Dynamics*. IAHR Monograph, Balkema, Rotterdam, 272 pp.

Davies, J.R., **Fletcher, C.J.N.**, **Waters, R.A.**, **Woodhall, D.G.** and **Zalasiewicz, J.A.** (1997) *Geology of the Country Around Llanilar and Rhayader*. Brit. Geol. Surv. Mem., Sheets 178 and 179 (England and Wales). Stationary Office, London.

Flemming, B.W. (2002) Geographic distribution of muddy coasts. In: *Muddy Coasts of the World Processes, Deposits and Function* (Eds Healy, T., Wang, Y. and Healy, J.A.), pp. 99–201. Elsevier, Amsterdam.

Fonnesu, M., **Haughton, P.**, **Felletti, F.** and **McCaffrey, W.** (2015) Short length-scale variability of hybrid event beds and its applied significance. *Mar. Petrol. Geol.*, **67**, 583–603.

Fonnesu, M., **Felletti, F.**, **Haughton, P.D.W.**, **Patacci, M.** and **Mccaffrey, W.D.** (2017) Hybrid event bed character and distribution linked to turbidite system sub-environments: The North Apennine Gottero Sandstone (north-west Italy). *Sedimentology*, **65**, 151–190.

Gingerich, P.D. (1969) Markov analysis of cyclic alluvial sediments. *J. Sed. Res.*, **39**, 330–332.

Gladstone, C., **McClelland, H.L.O.**, **Woodcock, N.H.**, **Pritchard, D.** and **Hunt, J.E.** (2018) The formation of convolute lamination in mud-rich turbidites. *Sedimentology*, **65**, 1800–1825.

Haughton, P.D.W., **Barker, S.P.** and **McCaffrey, W.D.** (2003) 'Linked' debrites in sand-rich turbidite systems – origin and significance. *Sedimentology*, **50**, 459–482.

Haughton, P.D.W., **Davis, C.**, **McCaffrey, W.** and **Barker, S.P.** (2009) Hybrid sediment gravity flow deposits – classification, origin and significance. *Mar. Petrol. Geol.*, **26**, 1900–1918.

Hodgson, D.M. (2009) Distribution and origin of hybrid beds in sand-rich submarine fans of the Tanqua depocentre, Karoo Basin, South Africa. *Mar. Petrol. Geol.*, **26**, 1940–1956.

Iverson, R.M. (1997) Physics of debris flows. *Rev. Geophys.*, **35**, 245–296.

Jobe, Z.R., **Lowe, D.R.** and **Morris, W.R.** (2012) Climbing-ripple successions in turbidite systems: depositional environments, sedimentation rates and accumulation times. *Sedimentology*, **59**, 867–898.

Jopling, A.V. and **Walker, R.G.** (1968) Morphology and origin of ripple-drift cross-lamination, with examples from the Pleistocene of Massachusetts. *J. Sed. Res.*, **38**, 971–984.

Kane, I.A. and **Pontén, A.S.M.** (2012) Submarine transitional flow deposits in the Paleogene Gulf of Mexico. *Geology*, **40**, 1119–1122.

Kane, I.A., **Pontén, A.S.M.**, **Vangdal, B.**, **Eggenhuisen, J.T.**, **Hodgson, D.M.** and **Spychala, Y.T.** (2017) The stratigraphic record and processes of turbidity current transformation across deep-marine lobes. *Sedimentology*, **64**, 1236–1273.

Kneller, B.C. and **Branney, M.J.** (1995) Sustained high-density turbidity currents and the deposition of thick massive sands. *Sedimentology*, **42**, 607–616.

Kneller, B. and **Buckee, C.** (2000) The structure and fluid mechanics of turbidity currents: a review of some recent studies and their geological implications. *Sedimentology*, **47**, 62–94.

Kneller, B. (1995) Beyond the turbidite paradigm: physical models for deposition of turbidites and their implications for reservoir prediction. In: *Characterisation of Deep Marine Clastic Systems* (Eds Hartley, A.J. and Prosser, D.J.), Geol. Soc. London Spec. Publ., **94**, 29–46.

Kneller, B., **Nasr-Azadani, M.M.**, **Radhakrishnan, S.** and **Meiburg, E.** (2016) Long-range sediment transport in the world's oceans by stably stratified turbidity currents. *J. Geophys. Res. Oceans*, **121**, 8608–8620.

Kuenen, P.H. and **Migliorini, C.I.** (1950) Turbidity currents as a cause of graded bedding. *J. Geol.*, **58**, 91–127.

Lovell, J.P.B. (1970) The palaeogeographical significance of lateral variations in the ratio of sandstone to shale and other features of the Aberystwyth Grits. *Geol. Mag.*, **107**, 147–158.

Lowe, D.R. (1988) Suspended-load fallout as an independent variable in the analysis of current structures. *Sedimentology*, **35**, 765–776.

Lowe, D.R. and **Guy, M.** (2000) Slurry-flow deposits in the Britannia Formation (Lower Cretaceous), North Sea: a new perspective on the turbidity current and debris flow problem. *Sedimentology*, **47**, 31–70.

Luchi, R., **Balachandar, S.**, **Seminara, G.** and **Parker, G.** (2018) Turbidity currents with equilibrium basal driving layers: a mechanism for long runout. *Geophys. Res. Lett.*, **45**, 1518–1526.

Marr, J.G., **Shanmugam, G.** and **Parker, G.** (2001) Experiments on subaqueous sandy gravity flows: the role of clay and water content in flow dynamics and depositional structures. *Geol. Soc. Am. Bull.*, **113**, 1377–1386.

McClelland, H.L.O., **Woodcock, N.H.** and **Gladstone, C.** (2011) Eye and sheath folds in turbidite convolute lamination: Aberystwyth Grits Group, Wales. *J. Struct. Geol.*, **33**, 1140–1147.

Mohrig, D. and **Marr, J.G.** (2003) Constraining the efficiency of turbidity current generation from submarine debris flows and slides using laboratory experiments. *Mar. Petrol. Geol.*, **20**, 883–899.

Pickering, K., **Stow, D.**, **Watson, M.** and **Hiscott, R.** (1986) Deep-water facies, processes and models: a review and classification scheme for modern and ancient sediments. *Earth-Sci. Rev.*, **23**, 75–174.

Pierce, C.S., **Haughton, P.D.W.**, **Shannon, P.M.**, **Pulham, A.J.**, **Barker, S.P.** and **Martinsen, O.J.** (2018) Variable character and diverse origin of hybrid event beds in a sandy

submarine fan system, Pennsylvanian Ross Sandstone Formation, western Ireland. *Sedimentology*, **65**, 952–992.

Piper, D.J.W., **Stow, D.A.V.** and **Normark, W.R.** (1984) The Laurentian Fan: Sohm Abyssal Plain. *Geo-Mar. Lett.*, **3**, 141–146.

Prélat, A., **Hodgson, D.M.** and **Flint, S.S.** (2009) Evolution, architecture and hierarchy of distributary deep-water deposits: a high-resolution outcrop investigation from the Permian Karoo Basin, South Africa. *Sedimentology*, **56**, 2132–2154.

Pyles, D.R. and **Jennette, D.C.** (2009) Geometry and architectural associations of co-genetic debrite-turbidite beds in basin-margin strata, Carboniferous Ross Sandstone (Ireland): applications to reservoirs located on the margins of structurally confined submarine fans. *Mar. Petrol. Geol.*, **26**, 1974–1996.

van Rijn, L.C. (1990) *Principles of Fluid Flow and Surface Waves in Rivers, Estuaries, Seas and Oceans*. AQUA Publications,, Amsterdam.

van Rijn, L.C. (1993) *Principles of Sediment Transport in Rivers, Estuaries and Coastal Seas*. AQUA Publications, Amsterdam.

Schindler, R.J., **Parsons, D.R.**, **Ye, L.**, **Hope, J.A.**, **Baas, J.H.**, **Peakall, J.**, **Manning, A.J.**, **Aspden, R.J.**, **Malarkey, J.**, **Simmons, S.**, **Paterson, D.M.**, **Lichtman, I.D.**, **Davies, A.G.**, **Thorne, P.D.** and **Bass, S.J.** (2015) Sticky stuff: redefining bedform prediction in modern and ancient environments. *Geology*, **43**, 399–402.

Shanmugam, G. and **Moiola, R.J.** (1995) Reinterpretation of depositional processes in a classic flysch sequence (Pennsylvanian Jackfork Group), Ouachita Mountains, Arkansas and Oklahoma. *AAPG Bull.*, **79**, 672–695.

Smith, R. (2004) Turbidite systems influenced by structurally induced topography in the multi-sourced Welsh Basin. In: *Confined Turbidite Systems* (Ed. Lomas, S.A.), Geol. Soc. London Spec. Publ., **222**, 209–228.

Spearman, J. and **Manning, A.J.** (2017) On the hindered settling of sand–mud suspensions. *Ocean Dyn.*, **67**, 465–483.

Sprague, A.R.G., **Garfield, T.R.**, **Goulding, F.J.**, **Beaubouef, R.T.**, **Sullivan, M.D.**, **Rossen, C.**, **Campion, K.M.**, **Sickafoose, D.K.**, **Abreu, V.**, **Schellpeper, M.E.**, **Jensen, G.N.**, **Jennette, D.C.**, **Pirmez, C.**, **Dixon, B.T.**, **Ying, D.**, **Ardill, J.**, **Mohrig, D.C.**, **Porter, M.L.**, **Farrell, M.E.** and **Mellere, D.** (2005) Integrated slope channel depositional models: the key to successful prediction of reservoir presence and quality in offshore West Africa. Colegio de Ingenieros Petroleros de Mexico, Veracruz, Mexico, pp. 1–13.

Spychala, Y.T., **Hodgson, D.M.**, **Prélat, A.**, **Kane, I.A.**, **Flint, S.S.** and **Mountney, N.P.** (2017) Frontal and lateral submarine lobe fringes: comparing sedimentary facies, architecture and flow processes. *J. Sed. Res.*, **87**, 75–96.

Stevenson, C.J., **Talling, P.J.**, **Masson, D.G.**, **Sumner, E.J.**, **Frenz, M.** and **Wynn, R.B.** (2014) The spatial and temporal distribution of grain-size breaks in turbidites. *Sedimentology*, **61**, 1120–1156.

Sumner, E.J., **Talling, P.J.** and **Amy, L.A.** (2009) Deposits of flows transitional between turbidity current and debris flow. *Geology*, **37**, 991–994.

Talling, P.J. (2001) On the frequency distribution of turbidite thickness. *Sedimentology*, **48**, 1297–1329.

Talling, P.J. (2013) Hybrid submarine flows comprising turbidity current and cohesive debris flow: deposits, theoretical and experimental analyses, and generalized models. *Geosphere*, **9**, 460–488.

Talling, P.J., **Amy, L.A.**, **Wynn, R.B.**, **Peakall, J.** and **Robinson, M.** (2004) Beds comprising debrite sandwiched within co-genetic turbidite: origin and widespread occurrence in distal depositional environments. *Sedimentology*, **51**, 163–194.

Talling, P.J., **Masson, D.G.**, **Sumner, E.J.** and **Malgesini, G.** (2012) Subaqueous sediment density flows: depositional processes and deposit types. *Sedimentology*, **59**, 1937–2003.

Wang, Z. and **Plate, E.C.H.J.** (1996) A preliminary study on the turbulence structure of flows of non-Newtonian fluid. *J. Hydraul. Res.*, **34**, 345–361.

Wilson, D., **Davies, J.**, **Walters, R.** and **Zalasiewicz, J.** (1992) A fault-controlled depositional model for the Aberystwyth Grits turbidite system. *Geol. Mag.*, **129**, 595–607.

Winterwerp, J.C. and **van, Kesteren, W.G.M.** (2004) *Introduction to the Physics of Cohesive Sediment Dynamics in the Marine Environment*. Dev. Sedimentol., 56, Elsevier, Amsterdam.

Wood, A. and **Smith, A.J.** (1958) The sedimentation and sedimentary history of the Aberystwyth Grits (Upper Llandoverian). *Q. J. Geol. Soc.*, **114**, 163–195.

Manuscript received 9 January 2019; revision accepted 27 January 2020